

1 Dear Editor-in-chief,

2

3 Thank you for the consideration of our manuscript. This file includes our previous point-
4 by-point response to the reviewers and the tracked changed version of our new
5 manuscript. The track changes to the supplementary file are also included at the end.

6

7 On behalf of the authors,

8 Chris Colose

9 We appreciate the time and effort by the referee in reviewing this manuscript. We will
10 address all issues, as highlighted below (reviewer text in red):

11
12 “The ITCZ shifts away from the hemisphere with greater forcing”- please specify that
13 you mean greater NEGATIVE or VOLCANIC forcing.

14
15 Agreed that this is improved phrasing, we will correct to “The ITCZ shifts away from the
16 hemisphere with greater volcanic forcing.”

17
18 Line 136- how many latitudinal bands does G08 use? Also line 144- could you add some
19 more detail about the G08 dataset and how it was derived- e.g. ice core based? And more
20 information about the aerosol transport model?

21 and,
22 Line 157 The stratospheric sulfate aerosol loadings given by G08 are a function of
23 latitude, altitude and month”- What resolution is G08 both horizontally and vertically?

24
25
26 The G08 dataset provides sulfate aerosol loading from 9 km to 30 km (at 0.5 km
27 resolution) for each 10° latitude belt (from 90°S to 90°N – i.e., 18 latitude bands). It is
28 indeed derived from ice core sulfate records. We will add more information in the revised
29 manuscript.

30
31 Line 140- “the impact of these smaller amplitude and slowly varying forcings is very
32 small.”- Did you test this, or is it speculation?

33
34 During the preparation of this paper, this was tested in single-forcing runs in CESM, and
35 also with multiple (simultaneous) forcings in the GISS model (each without volcanoes).
36 The “composite” results obtained by averaging over the same dates as in the volcano
37 composites are indistinguishable from noise, and averaging over hundreds of “events”
38 would produce a nearly blank anomaly map (white almost everywhere), due to averaging
39 out internal variability and the fact that any instance of solar or land-use forcing (relative
40 to a five year interval immediately prior) will be extremely small. If the analysis were
41 repeated in a control simulation, the results would be indistinguishable.

42
43 Line 154- is this at different levels in the stratosphere as well?

44
45 Yes– in the GISS model, there is an optical thickness from 15-35 km. We will make a
46 note of this in the revised text.

47
48 Line 175- How big is Pinatubo for comparison?

49 Pinatubo remains elevated at ~20-30 Tg sulfate aerosol in the G08 dataset for about a
50 year, and drops off to <1 Tg after 4-5 years. We will add this to the revised text.

51
52 Line 184- is there any reason for using MJJAS and NDJFM for the warm and cold season
53 rather than MJJASO and NDJFMA? I expect the results would be similar, but I’m just
54 intrigued!

55
56
57
58
59
60
61
62
63
64
65
66
67
68
69
70
71
72
73
74
75
76
77
78
79
80
81
82
83
84
85
86
87
88
89
90
91
92
93
94
95
96
97
98
99
100

In our analyses, we intended only to capture any sensitivity of the anomalous response to seasonality, and we feel our choice is appropriate for that target. In the early stages of the manuscript we did the analysis for DJF and JJA, and decided to expand the month range to include more of the data, but the conclusions did not change, and any differences were barely noticeable “by eye.”

Lines 217-218 – “The G08 reconstructions used a simple transport model that does not allow for cross-equatorial aerosol transport” –I’m a bit confused as to what exactly this means and what the implications are- does it mean that if an eruption happens one side of the equator that none of the aerosols go to the other side?

We apologize for the confusion, and will modify the text. Two datasets emerged from the G08 study, the first an aerosol injection dataset for each hemisphere (in mass units). The second dataset (used for forcing GCMs) provides latitude/altitude information of aerosol concentration, at the resolutions previously mentioned. In the second dataset, the spatial evolution was derived from a simple model that parameterizes transport between the tropics, extratropics, and poles, and they interpolated the vertical distribution of aerosols based on information from the Pinatubo eruption. Cross-equatorial transport of aerosol was not allowed, and so tropical eruptions that left an imprint in both Polar Regions were represented by separate aerosol injections in both hemispheres. This was done since the ice core estimates provide information on the hemispheric distribution of volcanic aerosols, information that could only be preserved in their setup if hemisphere-only transport was permitted.

It is true that these details influence the volcanic forcing in all of the CMIP5/PMIP3 (and CESM LME) runs that utilized G08, and we do not take a position in this paper on the realism of the reconstruction. Improvements in volcanic forcing are at the forefront of research on last millennium climate, and we expect advances in CMIP6. For our purposes, however, this does not matter since the different composites (ASYMM_{NH}, ASYMM_{SH}, SYMM) have been formed from a forcing distribution that was imposed on the GCM and is perfectly defined. Thus, while forcing uncertainty (either in timing, magnitude, or spatial structure) is an important consideration for connecting the model results with paleoclimate proxy data, the responses we report are self-consistent with the forcing.

Line 221- does this imply that Tambora has more aerosols in the NH than SH? Or that it is symmetrical. Can you be more specific?

Tambora is actually a SYMM event in our composites (and would be if we used the Crowley volcanic reconstruction as well), based on the criteria we used of a <25% ratio in hemispheric-mean aerosol loading. However, there are slightly more aerosols in the NH in G08 and slightly more in the SH in Crowley. We will clarify this, but the main point in making this statement was that there is uncertainty in the reconstructions.

101 Line 248 “In the ASYMMNH and SYMM results, the cooling peaks over the Eurasian
102 and North American continents.” - But not in SYMM MJJAS
103
104 This is correct, we will modify the text. Thank you.
105
106 Line 250: Mid latitudes? or is it more high latitudes? Maybe mid to high latitudes?
107
108 We will write “mid-to-high latitudes.” Thank you.
109
110 Line 264: “suggesting AET away from the forced hemisphere” Do you mean towards?
111
112 Yes, thank you for spotting this typo.
113
114 Line 271: “after normalizing each event by a common global aerosol mass excursion,
115 thereby accounting for differences in the average forcing among the different eruptions”.
116 Maybe add a caveat that this doesn’t take into account things like coagulation of aerosols
117 for bigger eruptions which tends to reduce climate effects for a given mass
118 of aerosols (see Timmreck et al 2009), and assumes that the response pattern scales
119 linearly. For ITCZ excursions, the end of the paper suggests that this is not the case for
120 asymmetric forcing- the ITCZ moves more for a bigger forcing gradient between
121 hemispheres.
122
123 Agreed on all points, thank you. We will modify the text to caution interpreting a
124 normalized metric in the presence of non-linear effects.
125
126 Line 288- does this alignment error affect all/many eruptions in this dataset? Or is it just
127 Laki?
128
129 Most eruptions are not impacted. There were a few smaller events that were also not
130 included or mis-aligned, described in
131 <http://climate.envsci.rutgers.edu/IVI2/IVI2Version2ReadMe.pdf> (all of the participating
132 models that used G08 used version one of this dataset). We will carefully check whether
133 any of our dates require a similar caveat as we did for Laki, which is a much larger and
134 more well-known NH (Icelandic) eruption.
135
136 Line 323- Maybe mention some more of the ENSO and volcano studies that have been
137 done in the past- Whether or not volcanoes influence ENSO was certainly a bit of a
138 controversial issue in the literature at one point. I am not totally up to date with the most
139 recent studies though. Line 336- how big is a 0.5 C El Nino anomaly compared to a
140 typical El Nino event in the model? (e.g. a 1 standard deviation event?) Also, is it
141 statistically significant?
142
143 We will add citations to the revised manuscript to improve the ENSO segment.
144
145 In CESM, the El Niño events are too large (relative to observed amplitudes over the
146 historical period) and a 0.5 °C anomaly is well within the model’s range of natural

147 variability. However, the composite results always represent an average over hundreds of
148 events, and the event mean stands out following volcanic eruptions (Figure S6). We will
149 improve the statistical justification for this conclusion in the revised manuscript. We
150 interpret the positive SST anomalies in the eastern Pacific (in the composite) as a forced
151 response, or equivalently, we argue that volcanoes pre-condition the system toward El
152 Niño conditions. We will clarify this in the text and in the presentation of Figure S6.

153
154 “Line 345- It might be helpful to remind the reader that Samalas is somewhere between
155 NH and SYMM.”

156
157 We will add a note to the revised text. Thank you.

158
159 Line 364 “[rivers] are a useful variable in the context of monitoring since they integrate
160 precipitation changes over time” – and space. I would have thought that rivers would be
161 more useful in integrating precipitation changes over space than over time?

162
163 We agree; we will re-phrase the sentence. Thank you.

164
165 Lines 371-393- I feel that these paragraphs disproportionately emphasise the regions
166 where streamflow increases, when it actually decreases in a lot of areas. Can you make it
167 more balanced? Line 383-384 In ASYMMSH, “the ITCZ moves northward, resulting in
168 reduced river flux in the Amazon sector and increases in the Niger of central/wester
169 Africa” This is true for summer, but river flow decreases over the Niger in winter.

170
171 We emphasized increases just because there is previous literature that reports declines in
172 riverflow following large eruptions, but we fully agree the discussion should be more
173 balanced. We will modify the text to highlight both increases and decreases in river flow.

174
175 Line 407- is it worth mentioning that there are factors that affect d18O in the process
176 of being incorporated into paleo archives from precipitation? Lines 426-417- could you
177 outline briefly how the amount and temperature effects work and in which direction they
178 affect d18O concentrations?

179
180 In this paper, we wish to avoid discussing/speculating on the proxy system itself (e.g.,
181 cave-specific sites, etc.), which is a further complication for paleoclimate. The aim here
182 was to highlight the large-scale imprint on d18O in precipitation following volcanic
183 eruptions.

184
185 We will add text to make clear the known d18O-T and d18O-P relationships. Thank you.

186
187 Line 455 “In regions where tropical South American precipitation does not exhibit very
188 large changes, such in the NDJFM SYMM composites, temperature may explain much
189 of the isotopic response, again consistent with findings in Colose et al. (2016).” Can
190 you specify in which direction and how temperature affects the isotopic response?

191
192 As above, we will revise the manuscript to make this explicit. Thank you.

193
194 Line 470-1:- are the arrows the right way round for the LW fluxes? They seem to be the
195 opposite way round to the SW ones.
196
197 There was a mistake in this section. We will modify the SW arrows. Thank you.
198
199 Line 509 “Moisture makes it more difficult for the tropical circulation to transport energy
200 poleward”. How?
201
202 In the tropics, the latent heat flux is towards the Equator owing to the transport of moist
203 air in the low-level branch of the Hadley circulation. The circulation that cools (warms)
204 the deep tropics (subtropics) by adiabatic expansion (compressional heating) also carries
205 latent heat equatorward.
206
207 Figure 1: It would be nice to be able to see the absolute size of the volcanoes as well as
208 the hemispheric contrast in aerosol loading- can you put in an extra time series? At the
209 moment a perfectly symmetrical eruption will not show up at all. The overlap between
210 the red and black lines also makes it difficult to see how big the black lines are in some
211 cases. Also- what does FSNTC stand for?
212
213 We agree. We will create a completely new figure 1 to also highlight the absolute size of
214 the eruptions and remove line overlap.
215
216 FSNTC is the name of the clear-sky net shortwave flux (at TOA) diagnostic in the CESM
217 (CAM) history fields. We will replace this for clarity.
218
219 Figure 2- I assume this is surface temperature? (Rather than temperature at a different
220 level in the atmosphere?)
221
222 Yes– all temperature plots (except the latitude-pressure 3-D temperature figure in the
223 supplemental) are for the surface. We will write this in a revised caption for clarity.
224
225 Figure 8 panel a- the legend is a bit small. Panels b and c- The colour of the thin lines is
226 confusing because they are not that similar to their corresponding thick line- e.g. the thin
227 orange lines look like they go with total AET rather than the dry component.
228 Also- what depth of ocean is this for? All of it? And: “Grey envelope corresponds to the
229 total AET anomaly vs. latitude in a control simulation using 50 realizations of a
230 composite formed from the same dates as the ASYMMNH results”- I am not sure I
231 entirely understand what you mean by this- are there 50 control runs? If there is only one
232 control run, how are there 50 realisations if the same dates are used each time?
233
234 Thank you for highlighting an error in the description. First, we will remove the
235 climatological ocean heat transport curve, since it is not part of our study. The poleward
236 heat transport was for the full ocean. We will make the colors of all lines on the anomaly
237 plots consistent with those used on the climatology plot, and improve the legend size.
238

239 There is only one control run. The anomalous transport plots show the post-volcanic
240 spread in AET and its dry/latent components (each line shows a different eruption after
241 averaging over the ensemble member dimension). The grey envelope and rectangles in
242 Figure 8b,c are there to illustrate that the post-volcanic response is typically larger than
243 would be expected if the analysis were repeated on a control simulation. To do this, we
244 selected 16 different two-year intervals (each expressed as an anomaly relative to the
245 previous five years) in the 850-1850 C.E. period, and averaged those 16 anomaly fields
246 together. This analysis produces a single line in the transport-latitude plane, which does
247 not collapse to zero due to the finite averaging size. Averaging over a larger number of
248 cases than 16 would suppress the spread further, essentially mimicking the effect of
249 having a larger ensemble. The analysis is repeated 50 times, in each case with a random
250 selection of years, in order to generate a spread in AET anomaly at each latitude. This is a
251 benefit of a long control run.

252

253 The value we used should be the size of the actual ensemble for comparison, which was
254 14 in the discussion manuscript (for this figure). Since then, additional ensemble
255 members have been released (now 17), so the analysis will be repeated and reflected in
256 all plots and in the discussion. We will improve the caption and discussion.

257

258 **Figure 9: Could panels a and b be on the same scales to make them more obviously**
259 **comparable?**

260

261 Yes, we will revise the figure. Thank you.

262

263 **Supplement figure S7- You don't mention what the box is showing.**

264

265 Thank you, this is the Niño 3.4 domain. We will insert this in the figure caption.

266

267 **Technical corrections: Line 226- you have missed Iles and Hegerl 2015 off the reference**
268 **list at the end.**

269 and,

270 **Line 454 – “such >AS< in the NDJFM SYMM composites”**

271

272 Thank you, we will modify the text and reference section accordingly.

273

274 We appreciate the time and effort by the referee in reviewing this manuscript. We will
275 address all issues, as highlighted below (reviewer text in red):
276
277 **Line 29-30: Revise “the isotopic composition of the ITCZ” to “the isotopic composition**
278 **of precipitation in the ITCZ”.**
279
280 Thank you for the suggestion– we will modify the text.
281
282 **Line 33-35: Revise the final sentence of the abstract (“for the testing of models against**
283 **paleoclimate evidence.”) to be more specific.**
284
285 We will change to, “Our results highlight the need for the careful consideration of the
286 spatial structure of volcanic forcing for interpreting volcanic signals in proxy records, and
287 therefore in evaluating the skill of Common Era climate model output.”
288
289 We will add an example figure in the supplementary along these lines for the Asian
290 monsoon, which exhibits a different response to our northern or southern volcano
291 categories.
292
293 **Line 75 (and elsewhere): Revise reference “Adam et al., 2016, in press” to “Adam et al.,**
294 **2016”**
295
296 Thank you, we will update the reference.
297
298 **Line 87: Remove semi-colon before references.**
299
300 Thank you for noticing this. It looks like an extra parenthesis needs to be removed.
301
302 **Line 89: Add “in” between “asymmetries” and “the”.**
303
304 Thank you, we will correct.
305
306 **Line 189-190: Are the previous five seasons or five years used as a reference period?**
307 **Both are mentioned.**
308
309 We will clarify. Anomalies are always with respect to the same time of year evaluated
310 (e.g., NDJFM is relative to the previous five NDJFM’s), otherwise the seasonal cycle
311 becomes part of the response. For figures showing the monthly evolution of some
312 variable (e.g., Figure S6), anomalies are with respect to the previous five Januaries,
313 Februaries, etc., or for annual-mean metrics (Figure 8-9) the reference period is the full
314 60-month interval prior to the eruption.
315
316 **Line 268: Remove “that these results are consistent with”, as it is unnecessary and**
317 **diminishes the clarity of the sentence.**
318
319 Thank you, we will re-word this part.

320
321 Line 281: “the ITCZ shift may result in” May result in or does result in? Has this been
322 specifically evaluated in your analysis?
323 and,
324 Line 282-283: Rephrase “since the precipitation signal is strongest moving with the
325 ITCZ”. Unclear what is meant here.
326
327 Yes, Figure 5 shows this. We will re-word the sentence with stronger language and
328 clarity, but the answer has eruption/ensemble member dependence and so cannot be made
329 into a general statement. More often than not, however, precipitation increases in the
330 hemisphere-mean when the ITCZ moves toward it. The mean is strongly sensitive to
331 what happens in the ITCZ domain itself (rather than e.g., extratropical precipitation
332 changes) since the amplitude of the anomaly is very large, and located in the deep tropics
333 where the grid cell areas are larger.
334
335 Line 291: Rephrase “and therefore we restrict the anomalous precipitation field to a
336 single season” to “and therefore we restrict the anomalous precipitation field to the same
337 season.”
338
339 Thank you for the improved edit.
340
341 Line 296-303: The reference to Fig. S8 is missing. I suggest revising or removing this
342 paragraph, as it does not seem to add any new substantive information to the discussion.
343
344 Thank you for pointing out that we missed the reference, we will edit the paragraph to
345 improve the presentation and connection to the animations.
346
347 Line 325: Replace “eruptions in Table 1, multiplied by 15 ensemble members” to “16
348 eruptions in Table 1, multiplied by 15 ensemble members”.
349 and,
350 Line 338: Suggest replacing “In addition” with “Consistent with the SST anomalies,”
351 and,
352 Lines 341-344: Suggest replacing “we argue that the El Niño tendency in CESM is a
353 forced response in ASYMMNH but otherwise depends on the state of internal variability
354 concurrent with a given eruption. This explains why no such ENSO response is
355 associated with” with “we argue that the El Niño tendency in CESM is a forced response
356 in ASYMMNH but otherwise depends on the state of internal variability concurrent with
357 a given eruption, as no such ENSO response is associated with...”
358
359 Agreed with all recommendations. Thank you.
360
361 Lines 432: Rephrase or revise figure reference. Figure S5 shows that the NH-SH zonally
362 precipitation asymmetry is correlated to the AOD gradient. It does not show a correlation
363 between (18Op) and P.
364
365 This is correct, thank you. We will clarify this part of the paper.

366
367 Line 466-467 (Eqn 3): Derive this equation from first principles, or provide a description
368 of how Eqn. 3 was derived (e.g. modify Eqn. 1 in Hwang and Frierson, GRL, 2010 to
369 include the storage term).
370
371 Thank you, we will add references to justify the equation.
372
373 Lines 523-527: Is this data shown? If not, state as such.
374
375 We did show the anomalous latent energy flux (lines 523-524) in Figure 8. We did not
376 explicitly show a regression between AETeq and EFE (524-527) and we will state this.
377
378 Lines 537-538: Unclear what is meant by “the anomalous precipitation response is still
379 coherent”. Rephrase to clarify.
380 and,
381 Lines 552-553: Replace “regressing the different events in all three categories together”
382 to “regressing the precipitation median against the AETeq for each eruption (after
383 averaging over ensemble members)”.
384 and,
385 Lines 552-554: Cite which figure this data is taken from. Also add the equation of the
386 regression lines and correlation coefficients in Fig. 9.
387
388 We agree with the above and will re-phrase and modify the text or figures accordingly.
389
390 Lines 565-574: It is unclear how to interpret the representation of the ITCZ shift
391 presented in Eqn. 7 (and the relationship between the ITCZ shift and AHTeq) without a
392 theoretically-constrained N. It doesn’t appear valid (or meaningful) to conclude that
393 “energetically, it is quite easy to move the ITCZ”, given that “the slope of the
394 relationship between ITCZ location and AETeq may vary by a factor of 4-5 depending on
395 the relationship used”. Further explanation and discussion of this issue is needed here.
396
397 Thank you. We will elaborate in the revised text, but we agree that it is difficult to
398 interpret the magnitude of ITCZ shifts in the absence of a well-defined ITCZ metric.
399 However, several past papers have reported such numbers, and so here we are
400 highlighting that the slope is sensitive to which metric one chooses. This is an attempt to
401 illuminate prior discussions and interpretations rather than offer a “best” N, which may
402 indeed turn out to not be a useful question.
403
404 Lines 574-575: The final sentence in this paragraph seems abrupt and out of place.
405 Consider adding a few sentences or a paragraph to summarize the findings of the energy
406 budget analysis.
407 Line 687: Replace “to” with “in”.
408 Line 690: Replace “Results shown” with “Results are shown”.
409 Lines 693-694: Replace “N=the number of events used in each category, consistent with
410 the number of listed events in Table 1 (multiplied by 15 for CESM and 3 for GISS-E2).”
411 with “N=the number of events used in each category (consistent with the number

412 of listed events in Table 1, multiplied by 15 ensemble members for CESM and 3
413 ensemble members for GISS-E2).”
414 Line 715: Replace “Ensemble/Eruption” with “Composite”
415 Lines 717-718: Replace “Lighter lines associated with the dry and latent components
416 indicate the eruption spread, each averaged over 14 ensemble members.” with “Lighter
417 lines represent individual eruptions, each averaged over 14 ensemble members.”
418 Fig. 2 and Fig. 4: Revise labels to be consistent with text. E.g. replace “North” and
419 “South” with “ASYMMNH” and “ASYMMSH”.
420 Fig. 9: Plot ITCZ shift on same y-axis range for each subplot for visual clarity. Add 1:1
421 line to bottom left plot for visual clarity. Add equation of regression lines and correlation
422 coefficients to upper subplots and bottom left subplot.
423
424 We agree with all recommendations and will modify the text and figures. Thank you for
425 the suggestions, and time spent to improve the language of the paper.
426

427
428
429

430 Hemispherically asymmetric volcanic forcing of tropical hydroclimate during the last
431 millennium

432

433 **Christopher M. Colose¹, Allegra N. LeGrande², Mathias Vuille¹**

434

435 [1] Dept. of Atmospheric & Environmental Sciences, University at Albany, SUNY,
436 Albany, NY 12222

437 [2] NASA Goddard Institute for Space Studies, New York, NY, 10025

438 Correspondence to: Christopher Colose (ccolose@albany.edu)

Chris Colose 7/17/2016 11:04 PM
Deleted: and water isotopologue variability

440 **Abstract**

441 Volcanic aerosols exert the most important natural radiative forcing of the last
442 millennium. State-of-the-art paleoclimate simulations of this interval are typically forced
443 with diverse spatial patterns of volcanic forcing, leading to different responses in tropical
444 hydroclimate. Recently, theoretical considerations relating the intertropical convergence
445 zone (ITCZ) position to the demands of global energy balance have emerged in the
446 literature, allowing for a connection to be made between the paleoclimate simulations and
447 recent developments in the understanding of ITCZ dynamics. These energetic
448 considerations aid in explaining the well-known historical, paleoclimatic, and modeling
449 evidence that the ITCZ migrates away from the hemisphere that is energetically deficient
450 in response to asymmetric forcing.

451 Here we use two separate general circulation model (GCM) suites of experiments
452 for the Last Millennium to relate the ITCZ position to asymmetries in prescribed volcanic
453 sulfate aerosols in the stratosphere and related asymmetric radiative forcing. We discuss
454 the ITCZ shift in the context of atmospheric energetics, and discuss the ramifications of
455 transient ITCZ migrations for other sensitive indicators of changes in the tropical
456 hydrologic cycle, including global streamflow. For the first time, we also offer insight
457 into the large-scale fingerprint of water isotopologues in precipitation ($\delta^{18}\text{O}_p$) in response
458 to asymmetries in radiative forcing.

459 The ITCZ shifts away from the hemisphere with greater [volcanic](#) forcing. Since
460 the isotopic composition of [precipitation in](#) the ITCZ is relatively depleted compared to
461 areas outside this zone, this meridional precipitation migration results in a large-scale
462 enrichment (depletion) in the isotopic composition of tropical precipitation in regions the

463 ITCZ moves away from (toward). [Our results highlight the need for careful consideration](#)
464 [of the spatial structure of volcanic forcing for interpreting volcanic signals in proxy](#)
465 [records, and therefore in evaluating the skill of Common Era climate model output.](#)

Chris Colose 7/8/2016 7:36 PM

Deleted: Our results highlight the need for careful consideration of the spatial structure of volcanic forcing for both impact assessments and for the testing of models against paleoclimate evidence.

471 **1. Introduction**

472

473 The ITCZ is the narrow belt of deep convective clouds and strong precipitation
474 that develops in the rising branch of the Hadley circulation. Migrations in the position of
475 the ITCZ have important consequences for local rainfall availability, drought and river
476 discharge, and the distribution of water isotopologues (e.g., $\delta^{18}\text{O}$ and δD , hereafter
477 simply referred to as water isotopes, with notation developed in section 3.3) that are used
478 to derive inferences of past climate change in the tropics.

479 Meridional displacements of the ITCZ are constrained by requirements of
480 reaching a consistent energy balance on both sides of the ascending branch of the Hadley
481 circulation (e.g., Kang et al., 2008, 2009; Schneider et al., 2014). Although the ITCZ is a
482 convergence zone in near-surface meridional mass flux, it is a divergence zone
483 energetically. The stratification of the tropical atmosphere is such that moist static energy
484 (MSE) is greater aloft than near the surface, compelling Hadley cells to transport energy
485 in the direction of their upper tropospheric flow (Neelin and Held, 1987). If the system is
486 perturbed with preferred heating or cooling in one hemisphere, the anomalous circulation
487 that develops resists the resulting asymmetry by transporting energy from the heated to
488 the cooled hemisphere. Conversely, meridional moisture transport in the Hadley
489 circulation is primarily confined to the low-level equatorward flow, so the response of the
490 tropical circulation to asymmetric heating demands an ITCZ migration away from the
491 hemisphere that is energetically deficient. Since the mean circulation dominates the
492 atmospheric energy transport (AET) in the vicinity of the equator, the recognition that the
493 ITCZ is approximately co-located with the latitude where meridional column-integrated

494 energy fluxes vanish has provided a basis for relating the mean ITCZ position to AET.
495 We note that this perspective focused on atmospheric energetics is distinct from one that
496 emphasizes sea surface temperature gradients across the tropics (Maroon et al., 2016).

497 This energetic framework has emerged as a central paradigm of climate change
498 problems, providing high explanatory and predictive power for ITCZ migrations across
499 timescales and forcing mechanisms (Donohoe et al., 2013; McGee et al., 2014; Schneider
500 et al., 2014). It is also a compelling basis for understanding why the climatological
501 annual-mean ITCZ resides in the northern hemisphere (NH); it has been shown that this
502 is associated with ocean heat transport, which in the prevailing climate is directed
503 northward across the equator (Frierson et al., 2013; Marshall et al., 2014). The energetic
504 paradigm also predicts an ITCZ response for asymmetric perturbations that arise from
505 remote extratropical forcing. This phenomenon is exhibited in many numerical
506 experiments, is borne out paleoclimatically, and has gradually matured in its theoretical
507 articulation (Chiang and Bitz, 2005; Broccoli et al., 2006; Kang et al., 2008, 2009;
508 Yoshimori and Broccoli, 2008, 2009; Chiang and Friedman, 2012; Frierson and Hwang,
509 2012; Bischoff and Schneider, 2014; Adam et al., 2016).

510 Thus far, however, little or only very recent attention has been given to the
511 relation between transient ITCZ migrations and explosive volcanism (although see Iles et
512 al., 2014; Liu et al., 2016, section 2). This connection has received recent consideration
513 using carbon isotopes in paleo-records (Ridley et al., 2015) or in the context of volcanic
514 and anthropogenic aerosol forcing in the 20th century (Friedman et al., 2013; Hwang et
515 al., 2013; Allen et al., 2015; Haywood et al., 2015). The purpose of this paper is to use

Chris Colose 7/10/2016 5:19 PM
Deleted: , in press

Chris Colose 7/8/2016 7:37 PM
Deleted: , in press

518 the energetic paradigm as our vehicle for interpreting the climate response in
519 paleoclimate simulations featuring explosive volcanism of varying spatial structure.

520 Much of the existing literature highlighting the importance of spatial structure in
521 volcanic forcing focuses on the problem of tropical vs. high-latitude eruptions and
522 dynamical ramifications of changing pole-to-equator temperature gradients (e.g., Robock,
523 2000; Stenchikov et al., 2002; Shindell et al., 2004; Oman et al., 2005, 2006; Kravitz and
524 Robock, 2011), which is a distinct problem from one focused on inter-hemispheric
525 asymmetries [in](#) the volcanic forcing. Furthermore, episodes with preferentially higher
526 aerosol loading in the southern hemisphere (SH) have received comparatively little
527 attention, probably due to the greater propensity for both natural or anthropogenic aerosol
528 forcing to be skewed toward the NH.

529 Here we show that it matters greatly over which hemisphere the aerosol loading is
530 concentrated and that this asymmetry in aerosol forcing has a first-order impact on
531 changes in the tropical hydrologic cycle, atmospheric energetics, and the distribution of
532 the isotopic composition of precipitation.

533

534 **2. Methods**

535

536 To illuminate how the spatial structure of volcanic forcing expresses itself in the
537 climate system, we call upon two state-of-the-art models that were run over the pre-
538 industrial part of the last millennium, nominally 850-1850 C.E. (hereafter, LM), the most
539 recent key interval identified by the Paleoclimate Model Intercomparison Project Phase 3
540 (PMIP3). An analysis of this time period is motivated by the fact that volcanic forcing is

Chris Colose 7/8/2016 8:40 PM

Deleted: (

542 the most important radiative perturbation during the LM (LeGrande and Anchukaitis,
543 2015; Atwood et al., 2016). Furthermore, the available input data that defines volcanic
544 forcing in CMIP5/PMIP3 feature a greater sample of events, larger radiative excursions,
545 and richer diversity in their spatial structure than is available over the historical period.
546 This allows for a robust composite analysis to be performed over this interval.

547 The two GCM's that we use as our laboratory are NASA GISS ModelE2-R
548 (hereafter, GISS-E2) and the Community Earth System Model Last Millennium
549 Ensemble (CESM LME, hereafter, just CESM). The GISS-E2 version used here is the
550 same as the non-interactive atmospheric composition physics version used in the CMIP5
551 initiative (called 'NINT' in Miller et al., 2014). CESM is a community resource that
552 became available in 2015 (Otto-Bliesner et al., 2016), employing version 1.1 of CESM
553 that consists of several component models each representing different aspects of the Earth
554 system; the atmospheric component is the Community Atmosphere Model version 5
555 (CAM5, see Hurrell et al., 2013), which in CESM features 1.9° latitude x 2.5° longitude
556 horizontal resolution with 30 vertical levels up to ~2 hPa. The GISS-E2 model is run at a
557 comparable horizontal resolution (2° x 2.5°) and with 40 vertical levels up to 0.1 hPa.

558 Both GISS-E2 and CESM feature multiple ensemble members that include
559 volcanic forcing. There are only a small number of volcanic eruptions in our different
560 forcing classifications (see below) in each 1000 year realization of the LM, motivating an
561 ensemble approach to sample multiple realizations of each eruption. There are currently
562 18 members in CESM, including 13 with all transient forcings during the LM and five
563 volcano-only simulations. This number is much higher than the number of ensembles
564 used for participating LM simulations in CMIP5/PMIP3. The volcanic reconstruction is

Chris Colose 7/15/2016 5:01 PM
Deleted: (NINT)

Chris Colose 7/17/2016 9:03 PM
Deleted: , in press

Chris Colose 7/15/2016 5:04 PM
Deleted: , which is

Chris Colose 7/15/2016 5:12 PM
Deleted: one of the motivations for our model choices, since

Chris Colose 7/15/2016 4:58 PM
Deleted: our different volcanic composites (see below) each sample a limited number of events within the LM

Chris Colose 7/15/2016 5:05 PM
Deleted: .

Chris Colose 7/9/2016 3:12 PM
Deleted: 15

Chris Colose 7/9/2016 3:12 PM
Deleted: ten

576 | based on Gao et al., (2008, [hereafter](#), G08) and the ensemble spread is generated from
577 | round off differences in the initial atmospheric state ($\sim 10^{-14}$ °C changes in the
578 | temperature field). Sampling many realizations of internal variability is critical in the
579 | context of volcanic eruptions given the different trajectories that can arise in the
580 | atmosphere-ocean system in response to a similar forcing (Deser et al., 2012).

Chris Colose 7/10/2016 6:32 PM

Deleted: (

581 | For GISS-E2, there exist six available members that include a transient volcanic
582 | forcing history. Here, however we use only the three simulations that utilize the G08
583 | reconstruction. This [was](#) done in order to composite over the same dates as the CESM
584 | events, [and because](#) the other volcanic forcing dataset that NASA explored in their suite
585 | of simulations (Crowley and Unterman, 2013) only provides data over four latitude
586 | bands, complicating inferences concerning hemispheric asymmetry. [Taken together, there](#)
587 | [are 21,000 years of simulation time in which to explore the post-volcanic response while](#)
588 | [probing both initial condition sensitivity and the structural uncertainty between two](#)
589 | [different models.](#) The three GISS-E2 members also differ in the combination of transient
590 | solar/land-use histories employed, but since our analysis focuses only on the immediate
591 | post-volcanic imprint, the impact of these smaller amplitude and slowly varying forcings
592 | is very small. [We tested this using the composite methodology developed below on no-](#)
593 | [volcano simulations with other single forcing runs \(in CESM\) or with combined forcings](#)
594 | [\(in GISS-E2\) and found the results to be indistinguishable from that of a control run \(not](#)
595 | [shown\).](#)

Chris Colose 7/15/2016 5:13 PM

Deleted: is

Chris Colose 7/15/2016 5:13 PM

Deleted: as well as the fact that

596 | In both GISS-E2 and CESM, the model response is a slave to the spatial
597 | distribution of the imposed radiative forcing, which was based on the aerosol transport
598 | model of G08, rather than the coupled model stratospheric wind field, thus losing

Chris Colose 7/15/2016 4:56 PM

Deleted: Taken together, there are 18,000 years of simulation time in which to explore the post-volcanic response while probing both initial condition sensitivity and the structural uncertainty between two different models.

607 potential insight into the seasonal dependence of the response that may arise in the real
608 world. For our purpose, however, this is a more appropriate experimental setup, since the
609 spatial structure of the forcing is implicitly known (Figure 1).

610 [The original G08 dataset provides sulfate aerosol loading from 9 km to 30 km \(at](#)
611 [0.5 km resolution\) for each 10° latitude belt. This reconstruction is based on sulfate peaks](#)
612 [in ice cores and a model of transport that determines the latitudinal, height, and time](#)
613 [distribution of the stratospheric aerosol.](#) In CESM, aerosols are treated as a fixed size
614 distribution in three levels of the stratosphere, which provide a radiative effect, including
615 shortwave scattering and longwave absorption. The GISS-E2 model is forced with
616 prescribed Aerosol Optical Depth (AOD) from 15-35 km, based on a linear scaling with
617 the G08-derived column volcanic aerosol mass (Stothers, 1984; Schmidt et al., 2011),
618 with a size distribution as a function of AOD as in Sato et al (1993) – thus altering the
619 relative long wave and shortwave forcing (Lacis et al, 1992; Lacis, 2015).

620 We note that the GISS-E2 runs forced with the G08 reconstruction in
621 CMIP5/PMIP3 were mis-scaled to give approximately twice the appropriate AOD
622 forcing, although the spatial structure of forcing in the model is still coherent with G08.
623 For this reason, we emphasize the CESM results in this study. However, we still choose
624 to examine the results from the GISS-E2 model for two reasons. First, we view this error
625 as an opportunity to explore the climate response to a wider range of hemispheric forcing
626 gradients, even though it comes at the expense of not being able to relate the results to
627 actual events during the LM. Secondly, the GISS-E2 LM runs were equipped with
628 interactive water isotopes (section 3.3). A self-consistent simulation of the isotope field in
629 a GCM is important, since it removes a degree of uncertainty in the error-prone

Chris Colose 7/8/2016 4:00 PM

Deleted: The stratospheric sulfate aerosol loadings given by G08 are a function of latitude, altitude and month.

633 conversion of isotopic signals into more fundamental climate variables. To our
634 knowledge, an explicit simulation of the isotopic distribution following asymmetries in
635 volcanic forcing has not previously been reported.

636 In our analysis, we classify volcanic events as “symmetric” (SYMM), and
637 “asymmetric” (ASYMM_X), where the subscript X refers to a preferred forcing in the
638 Northern Hemisphere (NH) or Southern Hemisphere (SH). Composites are formed from
639 all events within each of the three classifications in order to isolate the volcanic signal.
640 All events must have a global aerosol loading > 8 Tg (1 teragram = 10¹² g) averaged
641 over at least one five-month period to qualify as an eruption and enter the composite. [For](#)
642 [comparison, the 1991 Mt. Pinatubo eruption remains elevated at ~20-30 Tg sulfate](#)
643 [aerosol in the G08 dataset for about a year, and drops off to <1 Tg after 4-5 years.](#)

644 Events fall into the SYMM category if they have less than a 25% difference in
645 aerosol loading between hemispheres, while the ASYMM_{NH} events have an at least 25%
646 higher loading in the NH relative to the SH. The opposite applies to events falling into
647 the ASYMM_{SH} category. The dates for which these thresholds are satisfied are taken
648 from the original G08 dataset (Table 1), and thus the CESM and GISS-E2 composites are
649 formed using the same events despite the GISS-E2 mis-scaling and other differences in
650 model implementation.

651 Results are reported for the boreal warm season (averaged over the MJJAS
652 months) and cold season (NDJFM), [except for annual-mean results in Figures 8-9, or for](#)
653 [showing the progression of signals at monthly resolution \(Figure S6, S9-S12\).](#) For each
654 eruption, we identify the post-volcanic response by averaging the number of consecutive
655 seasons during which the above criteria are met, typically 1-3 years. All seasons for an

656 eruption lasting [longer](#) than one year are first averaged together to avoid over-weighting
657 its influence in the composite. [Anomalies are with respect to the corresponding time of](#)
658 [year during the five years prior to the eruption](#). For overlapping eruptions, the five years
659 prior to the first eruption are used instead. This relatively short reference period allows
660 creating composites that are unaffected by changes in the mean background state due to
661 low-frequency climate change during the LM. Composites for the SYMM, ASYMM_{NH},
662 and ASYMM_{SH} cases are then obtained for each season and model by averaging over all
663 anomaly fields within the appropriate classification, including all ensemble members. A
664 two-sided Student's t-test was applied to all composites in order to identify regions where
665 the anomalous signal is significantly different ($p < 0.05$) from the mean background
666 conditions.

667 In no case does the classification of a given eruption change over the duration of
668 the event, with the exception of the largest eruption (Samalas, 1258 C.E.), which
669 straddles the 25% asymmetry criterion ([SYMM and ASYMM_{NH}](#)) throughout the years
670 following the event. This eruption would project itself most strongly onto the symmetric
671 [composite](#) but may reasonably be classified as ASYMM_{NH} due to the greater absolute
672 aerosol loadings in the NH. Due to this ambiguity, we omit the Samalas event from our
673 main results. We note that there are far more asymmetric eruptions during the LM based
674 on our criteria than SYMM cases, most of which easily meet the two thresholds outlined
675 above. Because of this, the classification assigned to each event is quite robust to slightly
676 different criteria in defining the ratio (or differences) in hemispheric aerosol loading.
677 Since the asymmetric composites are formed from a relatively large number of events,
678 our results are insensitive to the addition or removal of individual eruptions that may be

Chris Colose 7/8/2016 8:50 PM

Deleted: more

Chris Colose 7/8/2016 8:55 PM

Deleted: We use the previous five seasons as a reference period to calculate an anomaly for each event

Chris Colose 7/9/2016 3:45 PM

Deleted: results

684 more ambiguous in their degree of asymmetry. However, the SYMM composites are
685 formed from only a few events, and are therefore more sensitive to each of the individual
686 eruptions that are included.

687 We stress that in this study we are agnostic concerning the actual location of
688 individual LM eruptions. Although aerosols from high-latitude eruptions tend to be
689 confined to the hemisphere in which the eruption occurs, tropical eruptions may also lead
690 to an asymmetric aerosol forcing, as happened during the eruptions of El Chichón and
691 Mt. Agung during the historical period. The timing, magnitude, and spatial footprint of
692 LM eruptions are important topics of research (see e.g., an updated reconstruction from
693 Sigl et al., 2015), and our composite should strictly be interpreted as a self-consistent
694 response to the imposed forcing in the model.

695 Similar approaches of stratifying volcanic events during the LM have only begun
696 to emerge in the literature (e.g., Liu et al., 2016). Iles and Hegerl (2015) showed the
697 CMIP5 multi-model mean precipitation response to a few post-1850 eruptions,
698 emphasizing the spatial structure of the aerosols (see their supplementary Figure S14) but
699 noted that it would be desirable for a greater sample of events in order to group by the
700 location of the aerosol cloud. The LM provides an appropriate setting for this.
701 Additionally, we add to these results by presenting a simulation of the water isotope
702 distribution following different volcanic excursions. We emphasize that we are screening
703 events by spatial structure and since different magnitude eruptions enter into the different
704 composites, a quantitative comparison of the different event classifications (or the two
705 models) is not our primary objective and would require a more controlled experiment.
706 Instead, we are reporting on the different composite responses as they exist in current LM

Chris Colose 7/9/2016 3:36 PM

Deleted: The G08 reconstructions used a simple transport model that does not allow for cross-equatorial aerosol transport, and the inferred asymmetry may not be coherent with other reconstructions (e.g., the Tambora eruption in 1815 features more aerosols in the SH than in the NH in the Crowley and Unterman (2013) reconstruction, which is not the case in G08)

Chris Colose 7/9/2016 3:36 PM

Deleted: and

Chris Colose 7/15/2016 5:27 PM

Deleted: is

Chris Colose 7/15/2016 5:27 PM

Deleted: an

Chris Colose 7/9/2016 3:36 PM

Deleted: updates

Chris Colose 7/9/2016 3:36 PM

Deleted: but

721 simulations, and highlight the emergent structure that arises from different choices in
722 how eruptions are sorted, much of which is shown to be scalable to different eruption
723 sizes and robust to choices of model implementation.

724

725 3. Results

726

727 3.1) Temperature, Precipitation and ENSO response

728

729 Figure 2 illustrates the composite temperature anomaly for each classification and
730 season in the CESM model. In both the ASYMM_{NH} and ASYMM_{SH} cases, the

731 hemisphere that is subjected to the strongest forcing is preferentially cooled. In the

732 ASYMM_{NH} results, the cooling peaks over the Eurasian and North American continents.

733 As expected, there tends to be a much larger response over land, as well as evidence of

734 NH winter warming in the mid-to-high latitudes, a phenomenon previously highlighted in

735 the literature and often associated with increased (decreased) pole-to-equator

736 stratospheric (mid-tropospheric) temperature gradients (Figure S1) and a positive mode

737 of the Arctic/North Atlantic Oscillation (Robock and Mao, 1992, 1995; Stenchikov et al.,

738 2002; Shindell et al., 2004; Ortega et al., 2015). This effect is weak in the ASYMM_{NH}

739 composite, likely because the maximal radiative forcing is located in the NH, offsetting

740 any dynamical response, but is present in the SYMM and ASYMM_{SH} composites in both

741 models (see Figure S2 for the GISS-E2 composite).

742 In the SH, cooling is muted by larger heat capacity associated with smaller land

743 fraction, with weak responses over the Southern Ocean while still exhibiting statistically

Chris Colose 7/17/2016 9:57 PM

Deleted: and SYMM

Chris Colose 7/17/2016 9:58 PM

Deleted: and

746 significant cooling in South America, South Africa, and Australia in all cases. In fact, the
747 cooling in the ASYMM_{SH} composites is largely confined to the tropics, in contrast to the
748 polar amplified pattern that is common to most climate change experiments. The cooling
749 in all categories is communicated vertically (Figure S1) and across the free tropical
750 troposphere, suggesting AET [toward](#) the forced hemisphere (section 3.4) for asymmetric
751 forcing.

752 The cooling in the GISS-E2 model (Figure S2), displays a very similar spatial
753 structure to CESM in all categories but with much greater amplitude due to the larger
754 forcing. We note that the composite-mean forcing [is similar between the four asymmetric](#)
755 [panels, but larger in the symmetric cases. In Figure 3, we show the hemispheric and](#)
756 [global average temperature response for both models after normalizing each event by a](#)
757 [common global aerosol mass excursion, thereby accounting for differences in the average](#)
758 [forcing among the different eruptions. This is done to highlight spread associated with](#)
759 [internal variability and model differences, and assumes the response pattern scales](#)
760 [linearly to global forcing, which is unlikely to be true across all events and for the two](#)
761 [models. Nonetheless, the gross features of the hemispheric contrast and reduction in](#)
762 global-mean temperature are shared between both models.

763 The CESM precipitation response is shown in Figure 4 (Figure S3 for GISS-E2).
764 For both the ASYMM_{NH} and ASYMM_{SH} cases, the ITCZ shows a robust displacement
765 away from the forced hemisphere. The precipitation reduction in the SYMM composites
766 is much less zonally coherent, instead featuring tropical-mean reductions in precipitation
767 and a slight increase toward the subtropics (see also Iles et al., 2013; Iles and Hegerl,
768 2014). Despite global cooling and reduced global evaporation (not shown), the ITCZ shift

Chris Colose 7/8/2016 4:38 PM

Deleted: away

Mathias Vuille 7/21/2016 12:10 PM

Deleted: from

Chris Colose 7/8/2016 9:33 PM

Deleted: that these results are consistent with,

Chris Colose 7/8/2016 9:37 PM

Deleted: T

774 in ASYMM_{NH} and ASYMM_{SH} tends to result in precipitation increases in the hemisphere
775 that is least forced (Figure 5), since the hemispheric-mean precipitation signal is largely
776 influenced by the ITCZ migration itself.

777 The ensemble spread in precipitation for a selected eruption (1762 C.E., NDJFM)
778 is shown in Figure S4, corresponding to the Icelandic Laki aerosol loading (a large
779 ASYMM_{NH} event). We note that the Laki eruption in Iceland actually occurred in 1783
780 C.E., but is earlier in our composite due to an alignment error in the first version of the
781 G08 dataset. Results are shown for the 1763 C.E. boreal winter only (the full composite
782 also includes 1762, see Table 1; Figure S4 also reports the winter 1763 Niño 3.4 anomaly
783 in surface temperature for each ensemble member, and therefore we restrict the
784 anomalous precipitation field to the same season). The ITCZ shift away from the NH is
785 fairly robust across the ensemble members, particularly in the Atlantic basin, although
786 internal variability still leads to large differences in the spatial pattern of precipitation,
787 notably in the central and eastern Pacific.

788 The monthly time-evolution of the composite temperature and precipitation
789 responses for the ASYMM_{NH} and ASYMM_{SH} cases can be viewed in an animation
790 (Figures S9-S12). The global and hemispheric difference in aerosol loadings is also
791 shown for each timestep (at monthly resolution) in the animations. When averaged over
792 the individual eruptions within each classification, the global aerosol mass loading
793 remains elevated above 8 Tg for nearly two years, coincident with the peak temperature
794 and precipitation response that begins to dampen out gradually and relaxes back to pre-
795 eruption noise levels after ~4-5 years. The seasonal migration of anomalous precipitation
796 in the ITCZ domain occurs in nearly the same sense as the meridional movement of

Chris Colose 7/8/2016 9:39 PM
Deleted: may
Chris Colose 7/8/2016 9:40 PM
Deleted: strongest moving with the
Chris Colose 7/8/2016 9:40 PM
Deleted: and because the area-weighted averages emphasize the tropics more than higher latitudes
Chris Colose 7/8/2016 9:40 PM
Deleted: .

Chris Colose 7/15/2016 5:35 PM
Deleted: also

Chris Colose 7/8/2016 9:05 PM
Deleted: and therefore we restrict the anomalous precipitation field to a single season

Chris Colose 7/20/2016 2:43 PM
Deleted: the
Chris Colose 7/19/2016 11:59 PM
Deleted:
Chris Colose 7/19/2016 11:58 PM
Deleted: monthly
Chris Colose 7/19/2016 11:58 PM
Deleted: anomaly
Chris Colose 7/19/2016 11:58 PM
Deleted: in

811 climatological rainfall, [highlighting important connections between the timing of the](#)
812 [eruption relative to the seasonal cycle of rainfall at a given location.](#)

813 In both CESM and GISS-E2, the ITCZ shift is approximately scalable to eruption
814 size. For both models, we define a precipitation asymmetry index, PAi (Hwang and
815 Frierson, 2013) in each season as the area-weighted NH tropical precipitation minus SH
816 tropical precipitation (extending to 20° latitude) normalized by the model tropical-mean
817 precipitation, i.e.,

818

$$PAi = \frac{P_{EQ-20^{\circ}N} - P_{20^{\circ}S-EQ}}{P_{20^{\circ}S-20^{\circ}N}} \quad (1)$$

819

820 Supplementary Figure S5 illustrates the relationship between PAi and the AOD
821 gradient between hemispheres (AOD is inferred for the CESM model by dividing the
822 aerosol loading by 75 Tg in each hemisphere, an approximate conversion factor to
823 compare the results with GISS-E2). The mis-scaling in GISS-E2 results in a wider range
824 of AOD gradients than occurs in CESM. Both models feature more tropical precipitation
825 in the NH (SH) during boreal summer (winter) in their climatology, with more
826 asymmetry in CESM during boreal summer. Interestingly, the most asymmetric events in
827 GISS-E2 (those that result in equatorward precipitation movements) can be sufficient to
828 produce more precipitation in the tropical winter hemisphere, thus competing with the
829 seasonal insolation cycle in determining the seasonal precipitation distribution.

830 The meridional ITCZ shift leads to a number of important tropical climate
831 responses. For example, an intriguing feature of the temperature pattern in Figure 2 is the
832 El Niño response that is unique to the $ASYMM_{NH}$ composites. This is unlikely to be a

833 residual feature of unforced variability, since there are 288 events in the ASYMM_{NH}
834 composites (16 eruptions in Table 1, multiplied by 18 ensemble members), significantly
835 more than in the other categories. The GISS-E2 temperature composite (Fig. S2) also
836 features a relatively weak cooling for ASYMM_{NH}, despite the very large radiative
837 forcing. [The relationship between ENSO and volcanic eruptions has, historically, been](#)
838 [quite complicated due to the problem of separating natural variability from the forced](#)
839 [response, and due to a limited sample of historical eruptions where ENSO events were](#)
840 [already underway prior to the eruption. Older studies have suggested that El Niño events](#)
841 [may be more likely 1 to 2 years following a large eruption \(e.g., Adams et al., 2003;](#)
842 [Mann et al., 2005; Emile-Geay et al., 2008\).](#) Our findings are also consistent with recent
843 results (Pausata et al., 2015) that found an El Niño tendency to arise from a Laki-like
844 forcing (in that study, a sequence of aerosol pulses in the high latitudes that was confined
845 to the NH extratropics), [and was recently explored in CESM LME by Stevenson et al.](#)
846 [\(2016\).](#) Pausata et al. (2015) attributed the El Niño development directly to a southward
847 ITCZ displacement. Since low-level converging winds are weak in the vicinity of the
848 ITCZ, a southward ITCZ displacement leads to weaker easterly winds (a westerly
849 anomaly) across the central equatorial Pacific. This was shown for a different model
850 (NorESM1-M) and experimental setup, but also emerges in the ASYMM_{NH} composite
851 results for CESM. Indeed, a composite anomaly of ~ 0.5°C emerges over the Niño 3.4
852 domain, lasting up to two years (Figure S6) with peak anomalies in the first two boreal
853 winters after an eruption. [Consistent with the SST anomalies,](#) a relaxation of the zonal
854 winds and re-distribution of water mass across the Pacific Ocean can be observed in the
855 ASYMM_{NH} composite response (Figure S7).

Chris Colose 7/23/2016 6:51 PM

Deleted: 240

Chris Colose 7/17/2016 10:39 PM

Deleted: 15

Chris Colose 7/19/2016 10:11 PM

Deleted: This finding

Chris Colose 7/19/2016 10:11 PM

Deleted: is

Chris Colose 7/8/2016 9:59 PM

Deleted: In addition

861 Since the ITCZ shift is a consequence of differential aerosol loading, [we argue](#)
862 [that the El Niño tendency in CESM is a forced response in ASYMM_{NH} but otherwise](#)
863 [depends on the state of internal variability concurrent with a given eruption, as no such](#)
864 [ENSO response is associated with the composite SYMM or ASYMM_{SH} composites,](#)
865 although we note that El Niño does tend to develop in response to the Samalas eruption
866 that was removed from our composite, and would strongly influence the interpretation of
867 the SYMM results due to the few events sampled (not shown, [though see Stevenson et](#)
868 [al., 2016](#)). However, we also caution that this version of CESM exhibits ENSO
869 amplitudes much larger than observations, and also features strong El Niño events with
870 amplitudes that are ~2 times larger than strong La Niña events even in non-eruption
871 years. Therefore, we choose not to further explore the dependence of our results on
872 ENSO phasing.

873 [Because the ITCZ responds differently to the three eruption classifications, there](#)
874 [are implications for best practices in assessing the skill of climate model output against](#)
875 [proxy evidence. For example, Anchukaitis et al. \(2010\) noted discrepancies between](#)
876 [well-validated tree-ring proxy reconstructions of eruption-induced drought in the Asian](#)
877 [monsoon sector and the precipitation response following volcanic eruptions derived from](#)
878 [the NCAR CSM 1.4 millennial simulation. However, we note that monsoonal rainfall](#)
879 [responds differently to ASYMM_{NH}, ASYMM_{SH}, or SYMM events in both GISS-E2 and](#)
880 [CESM. Figure S8 shows a histogram of boreal summer \(MJJAS\) Asian-Pacific rainfall](#)
881 [anomalies for all events in both models. ASYMM_{NH} and SYMM eruptions generally lead](#)
882 [to reductions in rainfall over the broad region averaged from 65°-150°E, 10°-40°N \(see](#)
883 [also the spatial patterns in Figure 4 for CESM and Figure S3 for GISS E2-R\). Because of](#)

Chris Colose 7/8/2016 10:00 PM

Deleted: we argue that the El Niño tendency in CESM is a forced response in ASYMM_{NH} but otherwise depends on the state of internal variability concurrent with a given eruption. This explains why no such

Chris Colose 7/8/2016 10:01 PM

Deleted: categories

890 [the southward ITCZ shift in ASYMM_{NH}, the most pronounced precipitation reductions](#)
891 [occur for events within this category. In contrast, for ASYMM_{SH} events, the northward](#)
892 [ITCZ shift and associated monsoon developments are such that precipitation changes are](#)
893 [relatively muted, and often the anomalies are positive.](#)

894

895 3.2) *River outflow*

896

897 An ITCZ shift away from the forced hemisphere will manifest itself in several
898 other components of the tropical hydroclimate system that are important to consider from
899 the standpoint of both impacts as well as the development of testable predictions. One
900 such important component of the hydrologic cycle is global streamflow, a variable that [is](#)
901 [related to](#) excessive or deficient precipitation over a catchment. Rivers are important for
902 ecosystem integrity, agriculture, industry, power generation, and human consumption.
903 Streamflow anomalies associated with volcanic forcing in observations and models have
904 previously been documented for the historical period (Trenberth and Dai, 2007; Iles and
905 Hegerl, 2015). Here, we discuss this variable in the context of our symmetric and
906 asymmetric composites.

907 The hydrology module of the land-component of CESM simulates surface and
908 subsurface fluxes of water, which serve as input into the CESM River Transport Model
909 (RTM). The RTM was developed to route river runoff downstream to the ocean or
910 marginal seas and enable closure of the hydrologic cycle (Oleson et al., 2010). The RTM
911 is run on a finer grid (0.5° x 0.5°) than the atmospheric component of CESM.

Chris Colose 7/17/2016 10:22 PM
Deleted: tends to correlate with

Chris Colose 7/17/2016 10:21 PM
Deleted: , and are a useful variable in the context of monitoring since they integrate precipitation changes over time

916 Figure 6 shows the river discharge anomalies in our different forcing categories.
917 The southward ITCZ shift in ASYMM_{NH} results in enhanced discharge in central and
918 southern South America, especially in the southern Amazon and Parana River networks.
919 These territories of South America, along with southern Africa and Australia are the
920 primary regions where land precipitation increases in the tropics for ASYMM_{NH}, and the
921 river flow in these areas tends to increase. Our results are also consistent with Oman et al.
922 (2006), who argue for a reduced Nile River level (northeastern Africa) following several
923 large high northern latitude eruptions, including Laki and the Katmai (1912 C.E.)
924 eruption. Their results were viewed through the lens of weakened African and Indian
925 monsoons associated with reduced land-ocean temperature differences; our composite
926 results suggest that regional precipitation reductions may also be part of a zonally
927 coherent precipitation shift.

928 In ASYMM_{SH}, the ITCZ moves northward, resulting in reduced river flux in the
929 Amazon sector and increases (reduction) in the Niger of central/western Africa during
930 boreal summer (boreal winter). Interestingly, the Nile flow is also reduced in this case,
931 although to a lesser extent, despite very modest precipitation increases during MJJAS for
932 a southern hemisphere biased aerosol forcing. There are also modest discharge increases
933 in southern Asia. However, there is simply very little land in regions where northward
934 ITCZ shifts result in enhanced precipitation, suggesting less opportunity for increases in
935 discharge to a SH biased eruption. For the SYMM eruptions, river discharge is reduced
936 nearly everywhere in the tropics, consistent with the precipitation reductions that occur
937 (Figure 3). The response is weaker or even reversed in the subtropics, such as in southern
938 South America, where precipitation tends to increase (Iles and Hegerl, 2015).

939

940 3.3) *Water isotopic variability*

941

942 Another important variable that integrates several aspects of the tropical climate
943 system is the isotopic composition of precipitation. Here, we focus on the relative
944 abundance of $^1\text{H}_2^{18}\text{O}$ versus the more abundant $^1\text{H}_2^{16}\text{O}$, commonly expressed as $\delta^{18}\text{O}$,
945 such that:

946

$$\delta^{18}O_p \equiv \left\{ VSMOW^{-1} \frac{O_{mp}^{18}}{O_{mp}^{16}} - 1 \right\} \times 1000 \quad (2)$$

947

948 where O_{mp}^{18} and O_{mp}^{16} are the moles of oxygen isotope in a sample, in our case
949 precipitation (denoted by the subscript mp). Delta values are with respect to the isotopic
950 ratio in a standard sample, the Vienna Standard Mean Ocean Water (VSMOW=
951 2.005×10^{-3}).

952 $\delta^{18}O_p$ is a variable that is directly obtained from many paleoclimate proxy
953 records. Therefore, rather than relying on a conversion of the local isotope signal to some
954 climate variable, the explicit simulation of isotopic variability is preferred for generating
955 potentially falsifiable predictions concerning the imprint associated with asymmetric
956 volcanic eruptions. Indeed, $\delta^{18}O_p$ variability is the result of an interaction between
957 multiple scales of motion in the atmosphere, the temperature of air in which the
958 condensate was embedded, and exchange processes operating from source to sink of the
959 parcel deposited at a site.

960 Water isotope tracers have been incorporated into the GISS-E2 model's
961 atmosphere, land surface, sea ice and ocean, and are advected and tracked through every
962 stage of the hydrologic cycle. A fractionation factor is applied at each phase change and
963 all freshwater fluxes are tagged isotopically. Stable isotope results from the lineage of
964 GISS-E2 models have a long history of being tested against observations and proxy
965 records (e.g., Vuille et al., 2003; Schmidt et al., 2007; LeGrande and Schmidt, 2008,
966 2009).

967 Figure 7 shows the $\delta^{18}O_p$ response in the GISS-E2 model. Seasonal calculations
968 are weighted by the precipitation amount for each month, although changes in the
969 seasonality of precipitation are not important in driving our results (not shown). The
970 literature on mechanistic explanations for isotope variability has a rich history of being
971 described by several "effects" such as a precipitation amount effect in deep convective
972 regions or a temperature effect at high latitudes (Dansgaard, 1964; Araguás-Araguás et
973 al., 2000), so named as to reflect the most important climatic driver of isotopic variability
974 at a site or climate regime. [Notably, \$\delta^{18}O_p\$ tends to be negatively correlated with](#)
975 [precipitation amount in the deep tropics and positively correlated with temperature at](#)
976 [high latitudes \(see e.g., Hoffman and Heimann, 1997 for a review of mechanisms\).](#)
977 However, [isotope-climate relations are generally complex. In our experiments, the \$\delta^{18}O_p\$](#)
978 [spatial pattern in the tropics \(Figure 7\) exhibits a similar pattern to](#) precipitation changes
979 induced by the ITCZ shift (Figure S5 for GISS-E2), particularly over the ocean. The
980 meridional movement of the ITCZ leads to an isotopic signal that is more positive
981 (enriched in heavy isotopes) in the preferentially forced hemisphere. The hemisphere
982 toward which the ITCZ is displaced on the other hand experiences increased tropical

- Chris Colose 7/19/2016 11:48 PM
Deleted: the isotopic
- Chris Colose 7/19/2016 11:47 PM
Deleted: response to volcanic eruptions is more complex than simply a response to one of these effects
- Chris Colose 7/19/2016 11:48 PM
Deleted: The
- Chris Colose 7/20/2016 2:51 PM
Deleted: is negatively correlated with

989 rainfall and a relative depletion of the heavy isotope (more negative $\delta^{18}O_p$). Thus, the
990 paleoclimatic fingerprint of asymmetric volcanic eruptions is characterized by a tropical
991 dipole pattern, with more positive (negative) $\delta^{18}O_p$ associated with reduced (increased)
992 rainfall.

993 Over land, South America stands out as exhibiting a palette of isotopic patterns
994 depending on forcing category and season. The South American monsoon system peaks
995 in austral summer, and the largest precipitation reductions occur in ASYMM_{SH} when the
996 ITCZ moves northward. There is a dipole pattern, characterized by isotopic enrichment
997 (depletion) in ^{18}O in the northern (southern) tropics of South America in ASYMM_{NH}
998 during NDJFM, while the opposite pattern emerges in ASYMM_{SH}, both associated with
999 Atlantic and east Pacific ITCZ displacements. During the austral winter, [climatological](#)
1000 South American precipitation peaks in the northern part of the continent, [and](#)
1001 precipitation [in this region](#) is reduced in both the SYMM and ASYMM_{SH} composites,
1002 leading to [a](#) large increase in $\delta^{18}O_p$. This is consistent with recent results in Colose et al.
1003 (2016), who used the isotope-enabled GISS-E2 model to form a composite of all large
1004 (AOD > 0.1) LM tropical volcanic events based on the Crowley and Unterman (2013)
1005 dataset. The eruptions analyzed in that study were smaller in amplitude due to differences
1006 in the scaling during implementation, as well as the fact that G08 tends to have larger
1007 volcanic events in the original dataset to begin with. In regions where tropical South
1008 American precipitation does not exhibit very large changes, such [as](#) in the NDJFM
1009 SYMM composites, temperature may explain much of the isotopic response, again
1010 consistent with findings in Colose et al. (2016).

1011

Chris Colose 7/19/2016 11:49 PM

Deleted: where

1013 3.4) Atmospheric Energetics

1014

1015 The overarching purpose of this work was to consider the influence of asymmetric
 1016 volcanic forcing on the energetic paradigm outlined in section 1. This framework of
 1017 analyzing ITCZ shifts in the context of asymmetric forcing predicts a net AET anomaly
 1018 toward the hemisphere that is preferentially forced by explosive volcanism, with anti-
 1019 correlated dry and latent energy fluxes both contributing to drive the ITCZ away from the
 1020 forced hemisphere. To examine this relationship in CESM, we first write a zonal-mean
 1021 energy budget for the atmosphere (Trenberth, 1997; Donohoe and Battisti, 2013):
 1022

$$\begin{aligned} & \frac{1}{2\pi a^2 \cos\phi} \frac{\partial AET}{\partial \phi} \\ & = ASR_{TOA} - OLR_{TOA} + SW_{sfc}^{\uparrow} - SW_{sfc}^{\downarrow} + LW_{sfc}^{\uparrow} - LW_{sfc}^{\downarrow} + LH_{sfc} \\ & + SH_{sfc} + L_f Sn - \frac{1}{g} \int_0^{p_s} \frac{\partial (c_p T + L_v q + k)}{\partial t} dp \quad (3) \end{aligned}$$

1023

1024 where ASR_{TOA} is the absorbed solar radiation, OLR_{TOA} is outgoing longwave
 1025 radiation at the top of the atmosphere (TOA), SW_{sfc}^{\uparrow} is reflected surface shortwave
 1026 radiation, SW_{sfc}^{\downarrow} is shortwave received by the surface (sfc), LW_{sfc}^{\uparrow} is longwave radiation
 1027 emitted (or reflected) by the surface, LW_{sfc}^{\downarrow} is longwave radiation received by the surface,
 1028 LH is the latent heat flux, SH is the sensible heat flux, Sn is snowfall rate, q is specific
 1029 humidity, k is kinetic energy, ϕ is latitude, a is the radius of the Earth, T is temperature,
 1030 c_p is specific heat capacity, L_v and L_f are the latent heats of vaporization and fusion, p is

Chris Colose 7/10/2016 3:20 PM

Deleted: ↓

Chris Colose 7/10/2016 3:20 PM

Deleted: ↑

1033 pressure ($p=p_s$ at the surface), and g is the acceleration due to gravity. All terms are
 1034 defined positive into the atmosphere, and the subscripts denote top-of-atmosphere (TOA)
 1035 or surface flux (sfc) diagnostics. Equation 3 effectively calculates MSE transport (section
 1036 1) as a residual of energy fluxes in the model.

1037 The last term ($\partial/\partial t$) on the right side of equation 3 is the time-tendency term,
 1038 representing storage of energy in the atmosphere (hereafter, $STOR_L$ and $STOR_D$ for latent
 1039 and dry energy, respectively). The time-derivative is calculated using finite differencing of
 1040 the monthly-mean fields. The term in the parentheses is the moist enthalpy, or MSE
 1041 minus geopotential energy. The kinetic energy is calculated in this study but is several
 1042 orders of magnitude smaller than other terms, and hereafter is folded into the definition of
 1043 $STOR_D$). The tendency term must vanish on timescales of several years or longer, but is
 1044 important in our context. We explicitly write out the snowfall term since CESM (and any
 1045 CMIP5 model) does not include surface energy changes associated with snow melt over
 1046 the ice-free ocean as part of the latent heat diagnostic, and must be calculated to close the
 1047 model energy budget.

1048 Integrating yields an expression for the atmospheric heat transport across a
 1049 latitude circle:

1050

$$AET(\phi) = 2\pi a^2 \int_{-\frac{\pi}{2}}^{\phi} (R_{TOA} + F_{sfc} - STOR_L - STOR_D) \cos \phi \, d\phi \quad (4)$$

1051 where we have combined the TOA terms into R_{TOA} and the snowfall and surface
 1052 diagnostics have collapsed into a single variable F_{sfc} . Similarly, the latent heat flux \mathcal{H}_L
 1053 across a latitude circle is:

$$\mathcal{H}_L(\phi) = 2\pi a^2 \int_{-\frac{\pi}{2}}^{\phi} (LH_{sfc} - L_v P - STOR_L) \cos \phi \, d\phi \quad (5)$$

1054 where P is precipitation in $\text{kg m}^{-2} \text{s}^{-1}$. We note that transport calculations are
 1055 presented for CESM and were done for only 17 ensemble members, since there are
 1056 missing output files for the requisite diagnostics in one run.

1057 Figure 8a shows the annual-mean climatological northward heat transport in
 1058 CESM, as performed by [the atmosphere](#), in addition to the [dry and moisture-related](#)
 1059 [components of AET](#). The total CESM climatological poleward transport is in good
 1060 agreement with observational estimates (e.g., Trenberth and Caron, 2001; Wunsch, 2005;
 1061 Fasullo and Trenberth, 2008), peaking at ~ 5.0 PW and ~ 5.2 PW in the SH and NH
 1062 subtropics, respectively (1 petawatt = 10^{15} W). In CESM, the SH receives slightly more
 1063 net TOA solar radiation than the NH (by $\sim 1.3 \text{ W m}^{-2}$ in the annual-mean), and the NH
 1064 loses slightly more net TOA longwave radiation to space (by $\sim 0.89 \text{ W m}^{-2}$). However, the
 1065 CESM annual ocean heat transport is northward across the equator ([not shown](#)), keeping
 1066 the NH warmer than the SH by ~ 0.98 °C. As a consequence, AET is directed southward
 1067 across the equator (red line). Moisture makes it more difficult for the tropical circulation
 1068 to transport energy poleward, and the transport of moisture in the low-level equatorward
 1069 flow is directed northward across the equator and associated with an annual-mean ITCZ
 1070 approximately co-located with the atmospheric energy flux equator (EFE), the latitude
 1071 where AET vanishes. This arrangement of the tropical climate is consistent with satellite
 1072 and reanalysis results for the present climate (Kang and Seager, 2012; Frierson et al.,
 1073 2013).

Chris Colose 7/17/2016 10:52 PM
 Deleted: 14

Chris Colose 7/23/2016 7:54 PM
 Deleted: both the atmosphere and ocean
 Chris Colose 7/23/2016 7:54 PM
 Deleted: latent component of the atmosphere

Chris Colose 7/21/2016 4:51 PM
 Deleted: Figure 8a, blue line
 Chris Colose 7/21/2016 6:46 PM
 Deleted: 97

1079 In response to asymmetric volcanic forcing, anomalous AET is directed toward
1080 the preferentially forced hemisphere (Figure 8b,c), along the imposed temperature
1081 gradient. Results are shown for the annual-mean AET anomaly in ASYMM_{NH} and
1082 ASYMM_{SH} for one year beginning with the January after each eruption, although
1083 averaging the first 2-3 years yields similar results with slightly smaller amplitudes. The
1084 equatorial AET (AET_{eq}) anomaly averaged over all events and ensemble members for
1085 ASYMM_{NH} (ASYMM_{SH}) is approximately 0.08 (-0.06) PW, defined positive northward,
1086 with much larger near-compensating dry and latent components. The anomalous moisture
1087 convergence drives the ITCZ shift away from the forced hemisphere. Anomalies in
1088 AET_{eq} when considering each unique volcanic event (after averaging over the 17
1089 ensemble members) are strongly anti-correlated with changes in the energy flux equator
1090 (r = -0.97, not shown), the latitude where AET vanishes.

Chris Colose 7/21/2016 9:41 PM

Deleted: 05

Chris Colose 7/17/2016 10:52 PM

Deleted: 14

Chris Colose 7/21/2016 4:43 PM

Deleted: 97

1091 The change in cross-equatorial energy transport for the SYMM ensemble/eruption
1092 mean (not shown) does not exhibit the coherence of the asymmetric cases for either AET
1093 or the individual dry and moist components, and in all cases does not emerge from
1094 background internal variability.

1095 Quantifying the ITCZ shift is non-trivial, since the precipitation field is less
1096 sharply defined than the EFE, and climate models (including the two discussed here)
1097 exhibit a bimodal tropical precipitation distribution (often called a “double-ITCZ”), often
1098 with one mode of higher amplitude in the NH (centered at 8°-9°N in CESM). However,
1099 despite pervasive biases that still exist in the climatology of tropical precipitation in
1100 CMIP5 (e.g., Oueslati and Bellon, 2015), the anomalous precipitation response is still
1101 characterized by a well-defined ITCZ shift (or a shift in the bimodal precipitation

Chris Colose 7/20/2016 3:14 PM

Deleted: coherent

1106 | [distribution, e.g., Figure 9 in Stevenson et al., 2016](#)) and the gross features presented here
1107 | are in agreement with theoretical considerations. In our analysis, a movement in the
1108 | latitude of maximum precipitation is not found to be a persuasive indicator of our ITCZ
1109 | shift. In fact, the meridional shift is better described as a movement in the center of mass
1110 | of the precipitation distribution, including changes in the relative amplitude of the two
1111 | modes (e.g., a heightening of the SH mode for a southward ITCZ shift). Different metrics
1112 | to describe the shift in the center of mass have been presented in the literature (e.g.,
1113 | Frierson and Hwang, 2012; Donohoe et al., 2013; Adam et al., 2016).

1114 | Here, we first adopt the precipitation median ϕ_{med} definition (e.g., Frierson and
1115 | Hwang, 2012) defined as the latitude where area-weighted precipitation from 20°S to
1116 | ϕ_{med} equals the precipitation amount from ϕ_{med} to 20°N, i.e., where the following is
1117 | satisfied:

$$\int_{20^{\circ}\text{S}}^{\phi_{\text{med}}} P \cos(\phi) d\phi = \int_{\phi_{\text{med}}}^{20^{\circ}\text{N}} P \cos(\phi) d\phi \quad (6)$$

1119 |
1120 | When considering the spread across eruption size (regressing the different events
1121 | in all three categories together after averaging over ensemble members) we find a
1122 | movement of $\sim -8.9^{\circ}$ shift in ITCZ latitude per 1 PW of anomalous AET_{eq} ([Figure 9](#)). The
1123 | sign of this relationship is a robust property of the present climate system, although [it is](#)
1124 | higher than other estimates (Donohoe et al., 2013) that analyzed the ITCZ scaling with
1125 | AET_{eq} to a number of other time periods and forcing mechanisms (not volcanic),
1126 | including the seasonal cycle, CO₂ doubling, Last Glacial Maximum, and mid-Holocene.

Chris Colose 7/19/2016 9:57 PM

Deleted: , in press

Chris Colose 7/21/2016 10:30 PM

Deleted: 4.7

Chris Colose 7/23/2016 5:17 PM

Deleted: it is slightly

1130 It was argued in that paper that the ITCZ is “stiff” in the sense that a large AET_{eq} is
 1131 required to move the ITCZ. However, the sensitivity of this relationship may vary
 1132 considerably depending on ITCZ metric considered (Figure 9 presents a scaling with
 1133 different indices), based on the following equation (Adam et al., 2016):

$$\phi_{ITCZ} = \frac{\int_{20^{\circ}S}^{20^{\circ}N} \phi (P \cos(\phi))^N d\phi}{\int_{20^{\circ}S}^{20^{\circ}N} (P \cos(\phi))^N d\phi} \quad (7)$$

1135
 1136 Here, N controls the weighting given to the modes in the precipitation
 1137 distribution. Typically, ϕ_{ITCZ} moves toward the precipitation maximum as N increases, but
 1138 importantly, the sensitivity of a ϕ_{ITCZ} migration to a given anomaly in AET_{eq} also
 1139 changes. Figure 9 shows the regression of anomalous ϕ_{med} and ϕ_{ITCZ} ($N = 5$) against
 1140 anomalous AET_{eq}. ($r = -0.94$), ϕ_{ITCZ} ($N = 3$) yields a high correlation ($r = -0.95$) and best
 1141 follows a 1:1 line with the EFE (Figure 9, bottomleft). The slope of the relationship
 1142 between ITCZ location and AET_{eq} may vary by a factor of 4-5 depending on the
 1143 relationship used. For example, there is approximately a -11.7° shift in ITCZ latitude per
 1144 1 PW of anomalous AET_{eq} using ϕ_{ITCZ} ($N = 3$). Thus, we interpret our results as
 1145 suggesting that energetically, it is not necessarily difficult to move the ITCZ, and urge
 1146 caution in characterizing past ITCZ shifts as being difficult to reconcile with paleo-
 1147 forcing estimates (Donohoe et al., 2013). Indeed, as many studies have used a
 1148 “precipitation centroid” or a similar variant to quantify tropical precipitation migrations,
 1149 we recommend exploring the sensitivity of ITCZ shifts to different ways of
 1150 characterizing the movement in precipitation mass unless the community can agree upon

- Chris Colose 7/19/2016 9:57 PM
Deleted: , in press
- Chris Colose 7/20/2016 3:17 PM
Deleted: ,
- Chris Colose 7/20/2016 3:17 PM
Deleted: typically
- Chris Colose 7/20/2016 3:17 PM
Deleted: moving
- Chris Colose 7/23/2016 7:06 PM
Deleted: also changing the
- Chris Colose 7/20/2016 3:17 PM
Deleted: the ITCZ shift
- Chris Colose 7/20/2016 3:17 PM
Deleted: to
- Chris Colose 7/23/2016 7:11 PM
Deleted: external forcing
- Chris Colose 7/23/2016 7:07 PM
Deleted: .
- Chris Colose 7/23/2016 7:07 PM
Deleted:
- Mathias Vuille 7/21/2016 1:52 PM
Comment [1]: ‘while’ does not seem appropriate here. Maybe separate into two sentences.
- Chris Colose 7/23/2016 7:12 PM
Deleted: N = 5 with
- Chris Colose 7/21/2016 10:58 PM
Deleted: 93
- Chris Colose 7/23/2016 7:10 PM
Deleted: while
- Chris Colose 7/23/2016 7:12 PM
Deleted: yielded the highest correlation
- Chris Colose 7/23/2016 7:13 PM
Deleted: , and in our case is
- Chris Colose 7/23/2016 7:13 PM
Deleted: their
- Chris Colose 7/20/2016 3:18 PM
Deleted: quite easy to
- Chris Colose 7/23/2016 7:15 PM
Deleted: s

1169 | [a well-defined “N” that suitably characterizes the precipitation distribution in both](#)
1170 | [climate models and observations.](#)

1171

1172 4. Conclusions

1173

1174 In this work, we have examined two models, NASA GISS ModelE2-R and the
1175 recently completed CESM Last Millennium Ensemble, and stratified volcanic events by
1176 their degree of asymmetry between hemispheres. We find a robust ITCZ shift away from
1177 the preferentially forced hemisphere, as a consequence of adjustments in the Hadley
1178 circulation that transports anomalous energy into the cooled hemisphere.

1179 An important component of our work was using the GISS-E2 model to explicitly
1180 simulate the oxygen isotopic imprint following major volcanic eruptions with asymmetric
1181 aerosol forcing. The ITCZ shift following asymmetric forcing leads to a more positive
1182 isotopic signal in the tropical regions the ITCZ migrates away from, and a relative
1183 depletion in heavy isotopes in regions the ITCZ migrates to. These results provide a
1184 framework for the search of asymmetric volcanic signals in high-resolution isotopic or
1185 other temperature and precipitation sensitive proxy data from the tropics.

1186 There is still considerably uncertainty in the timing and magnitude of LM
1187 eruptions. Improvements in particle size representation have been identified as critical
1188 target for improved modeling and comparisons to proxy data (e.g., G. Mann et al., 2015).
1189 Here, we argue that the inter-hemispheric asymmetry of the aerosol forcing also emerges
1190 as being of first-order importance for the expected volcanic response. Future
1191 developments in model-proxy comparisons should probe the uncertainty space not just in

Chris Colose 7/20/2016 3:21 PM
Deleted: . Therefore, probing uncertainties in the spatial structure in forcing must be of first-order consideration for credible paleoclimate simulations.

1196 the global-mean radiative forcing and coincident internal variability at the time of the
1197 eruption, but also the spatial structure of the aerosol cloud. For example, simulations that
1198 represent volcanic forcing simply as an equivalent reduction in total solar irradiance at
1199 the TOA are unrealistic and cannot be expected to be faithful to tropical climate proxy
1200 records.

1201 We hope this contribution will help motivate the connection between the spatial
1202 structure of volcanic episodes and the expression on tropical hydroclimate as an urgent
1203 paleoclimate target in future studies and model intercomparisons. Such investigation also
1204 calls for high-resolution and accurately dated tropical proxy networks that reach across
1205 hemispheres. Developments in seasonally and annually resolved volcanic reconstructions
1206 from both hemispheres (Sigl et al., 2015) are of considerable importance in such
1207 assessments. Future modeling efforts that are forced with the explicit injection of
1208 volcanic species, while also probing multiple realizations of internal variability that will
1209 dictate the spatio-temporal evolution of the volcanic aerosol, are also urgently required as
1210 a tool for understanding both past and future volcanic impacts.

1211

1212

1213 **Acknowledgments**

1214 This study was funded by NOAA C2D2 NA10OAR4310126 and NSF awards AGS-
1215 1003690 and AGS-1303828. We would like to thank NASA GISS-E2 for institutional
1216 support. Computing resources supporting this work were provided by the NASA High-
1217 End Computing (HEC) Program through the NASA Center for Climate Simulation
1218 (NCCS) at Goddard Space Flight Center. We acknowledge the CESM1(CAM5) Last

1219 Millennium Ensemble Community Project and supercomputing resources provided by
1220 NSF/CISL/Yellowstone.
1221

1222 **Figure Captions**

1223 **Figure 1.** [Global Aerosol Loading \(Tg\) from Gao et al. \(2008\) in red line. ASYMM_{NH}](#)
1224 [\(green circles\), ASYMM_{SH} \(blue circles\), and SYMM \(black circles\) events that are used](#)
1225 [in composites are shown. Note that Samalas is omitted, as discussed in text. The time-](#)
1226 [series is at seasonal \(five-month\) resolution and thus multiple points may be associated](#)
1227 [with a single eruption. The hemispheric contrast \(NH minus SH\) clear-sky net solar](#)
1228 [radiation \(FSNTC– in W/m²\) in CESM LME is shown in orange \(offset to have zero](#)
1229 [mean\).](#)

1230
1231 **Figure 2.** CESM spatial composite of [surface](#) temperature anomaly (°C) for (top row)
1232 ASYMM_{NH}, (middle row) ASYMM_{SH}, and (bottom row) SYMM events, each in (left
1233 column) NDJFM and (right column) MJJAS. Stippling indicates statistical significance
1234 using a two-sided student's t-test ($p < 0.05$).

1235
1236 **Figure 3.** [Box-and-whisker diagrams showing the \(red fill\) global mean, \(green fill\) NH](#)
1237 [mean, and \(blue fill\) SH mean temperature anomaly in the ASYMM_{NH}, ASYMM_{SH}, and](#)
1238 [SYMM eruption cases on vertical axis. All events are normalized by a 20 Tg global](#)
1239 [loading size. For GISS-E2, loadings were multiplied by a factor of two to approximately](#)
1240 [account for the over-inflated forcing prior to analysis. Results are shown for the CESM](#)
1241 [and GISS-E2 model and for NDJFM and MJJAS, as labeled. Black solid line indicates](#)
1242 [the median, box width spans the 25-75% quartiles, and tails span the full interval for all](#)
1243 [cases. N=the number of events used in each category \(consistent with the number of](#)
1244 [listed events in Table 1, multiplied by 18 ensemble members for CESM and 3 ensemble](#)

Chris Colose 7/9/2016 11:37 PM

Deleted: Annual-mean Northern Hemisphere minus Southern Hemisphere Aerosol Loading (Tg) from Gao et al. (2008) in black, and clear-sky net solar radiation (W/m²) in CESM LME in red (offset to have zero mean).

1250 [members for GISS-E2\). Bottom panels \(CTRL\) show the spread of 100 randomly](#)
1251 [selected and non-overlapping events averaged over two seasons \(relative to the previous](#)
1252 [five seasons\) in a control run.](#)

1253

1254 **Figure 4.** As in Figure 2, except for precipitation (mm/day).

1255

1256 **Figure 5.** As in Figure 3, except for precipitation (mm/day, normalized to 20 Tg in the
1257 forced simulations; mm/day in the control). N (not shown) is the same as in Figure 3.

1258

1259 **Figure 6.** As in Figures 2 and 4, except for river discharge (m^3/s , or 10^{-6} Sverdrups).

1260

1261 **Figure 7.** GISS-E2 spatial composite of the oxygen isotope anomaly (per mil) in (top
1262 row) ASYMM_{NH}, (middle row) ASYMM_{SH}, and (bottom row) SYMM events in (left
1263 column) NDJFM and (right column) MJJAS.

1264

1265 **Figure 8.** [a\) CESM climatology of atmospheric energy transport \(PW, black\), dry \(red\),](#)
1266 [and latent \(dark blue\) transports. b\) Composite mean anomaly in atmospheric heat](#)
1267 [transport for ASYMM_{NH} eruptions in total \(black\), dry \(red\), and latent \(blue\)](#)
1268 [components. Lighter \(orange and aqua\) lines represent individual eruptions, each](#)
1269 [averaged over 17 ensemble members. c\) As in \(b\), except for ASYMM_{SH} eruptions. Grey](#)
1270 [envelope corresponds to the total AET anomaly vs. latitude in a control simulation using](#)
1271 [50 realizations of a 17-event composite \(17 “events” with no external forcing,](#)
1272 [corresponding to the size of the ensemble\). Vertical bars correspond to the range of](#)

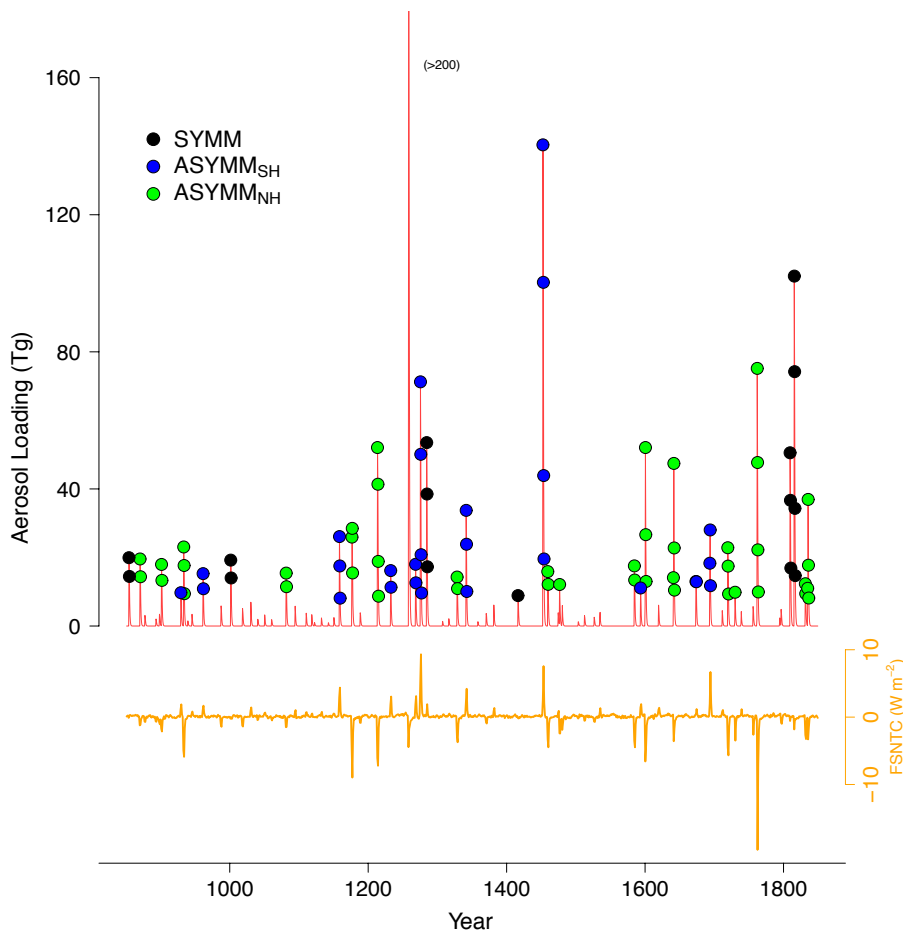
1273 | [\(aqua\) latent and \(orange\) dry components of cross-equatorial energy transport \(\$AET_{eq}\$ \) in](#)
1274 | [the control composite.](#)

1275

1276

1277 | **Figure 9.** [Annual-mean ITCZ shift represented by changes in \(topleft\) \$\phi_{med}\$, and](#)
1278 | [\(topright\) \$\phi_{ITCZ}\$ \(\$N = 5\$ \) vs. change in \$AET_{eq}\$. Changes in \$\phi_{ITCZ}\$ \(\$N = 3\$ \) vs. change in](#)
1279 | [EFE \(bottomleft\). See text for definitions. Total AET vs. latitude for a small band](#)
1280 | [centered around the equator for all volcanic events in \(green\) \$ASYMM_{NH_2}\$, \(blue\)](#)
1281 | [\$ASYMM_{SH_2}\$, and \(black\) SYMM cases \(bottomright\). Black dashed line indicates](#)
1282 | [climatological or pre-eruption AET values \(different choices are indistinguishable\).](#)
1283 | [Colored arrows represent the direction of anomalous \$AET_{eq}\$.](#)

1284



1285

1286 **Figure 1.** Global Aerosol Loading (Tg) from Gao et al. (2008) in red line, ASYMM_{NH}
 1287 (green circles), ASYMM_{SH} (blue circles), and SYMM (black circles) events that are used
 1288 in composites are shown. Note that Samalas is omitted, as discussed in text. The time-
 1289 series is at seasonal (five-month) resolution and thus multiple points may be associated
 1290 with a single eruption. The hemispheric contrast (NH minus SH) clear-sky net solar
 1291 radiation (FSNTC— in W/m²) in CESM LME is shown in orange (offset to have zero
 1292 mean).

Chris Colose 7/9/2016 11:31 PM

Deleted: Annual-mean Northern Hemisphere minus Southern Hemisphere

Chris Colose 7/9/2016 11:32 PM

Deleted: black

Chris Colose 7/9/2016 11:32 PM

Deleted: ,

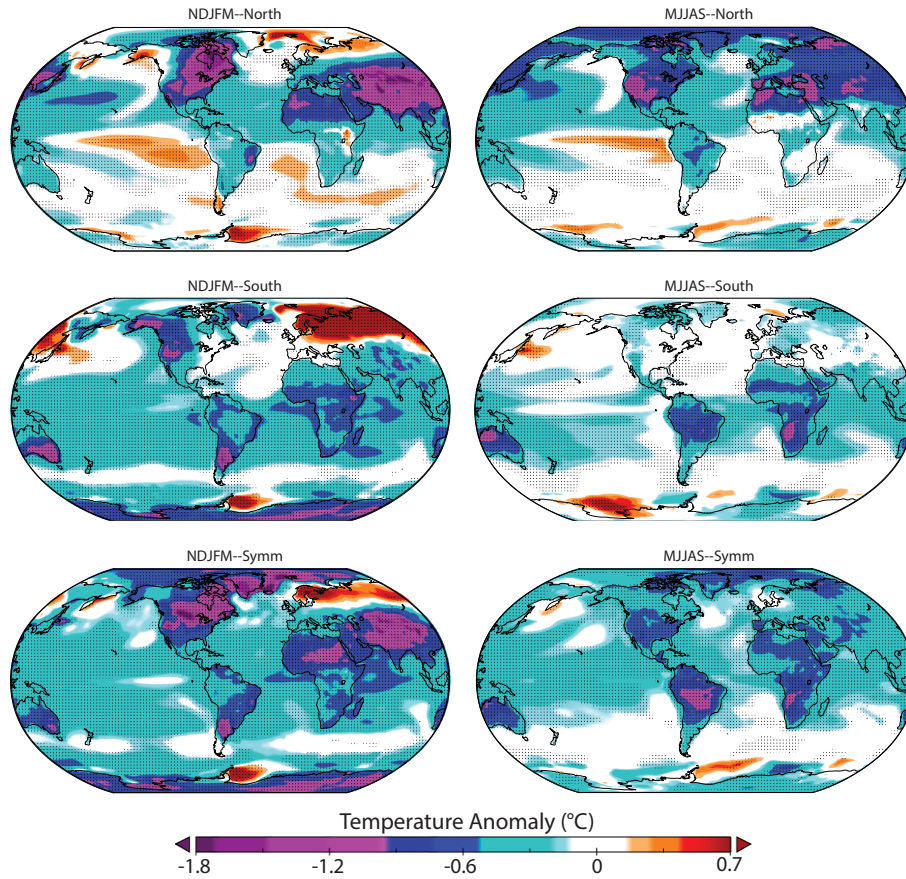
Chris Colose 7/9/2016 11:36 PM

Deleted: and

Chris Colose 7/9/2016 11:36 PM

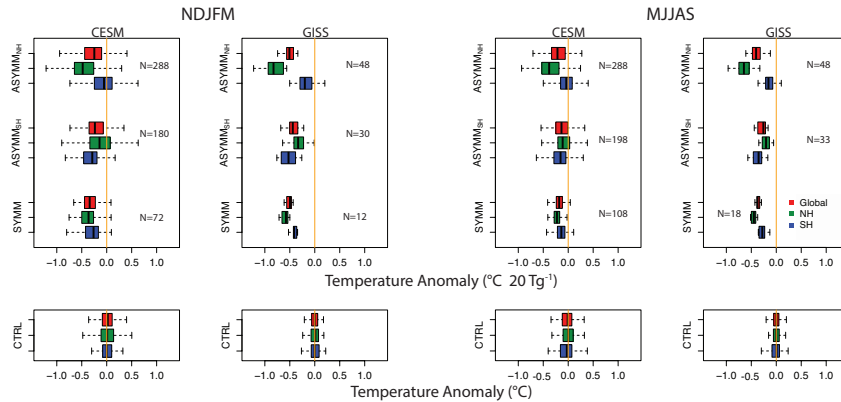
Deleted: n red

Temperature (Ensemble/Event Mean)



1299
1300
1301
1302
1303

Figure 2. CESM spatial composite of [surface](#) temperature anomaly (°C) for (top row) ASYMM_{NH}, (middle row) ASYMM_{SH}, and (bottom row) SYMM events, each in (left column) NDJFM and (right column) MJJAS. Stippling indicates statistical significance using a two-sided student's t-test ($p < 0.05$).



1304
 1305 **Figure 3.** Box-and-whisker diagrams showing the (red fill) global mean, (green fill) NH
 1306 | mean, and (blue fill) SH mean temperature anomaly [in](#) the ASYMM_{NH}, ASYMM_{SH}, and
 1307 | SYMM eruption cases on vertical axis. All events are normalized by a 20 Tg global
 1308 | loading size. For GISS-E2, loadings were multiplied by a factor of two to approximately
 1309 | account for the over-inflated forcing prior to analysis. Results [are](#) shown for the CESM
 1310 | and GISS-E2 model and for NDJFM and MJJAS, as labeled. Black solid line indicates
 1311 | the median, box width spans the 25-75% quartiles, and tails span the full interval for all
 1312 | cases. [N=the number of events used in each category \(consistent with the number of](#)
 1313 | [listed events in Table 1, multiplied by 18 ensemble members for CESM and 3 ensemble](#)
 1314 | [members for GISS-E2\)](#). Bottom panels (CTRL) show the spread of 100 randomly
 1315 | selected and non-overlapping events averaged over two seasons (relative to the previous
 1316 | five seasons) in a control run.

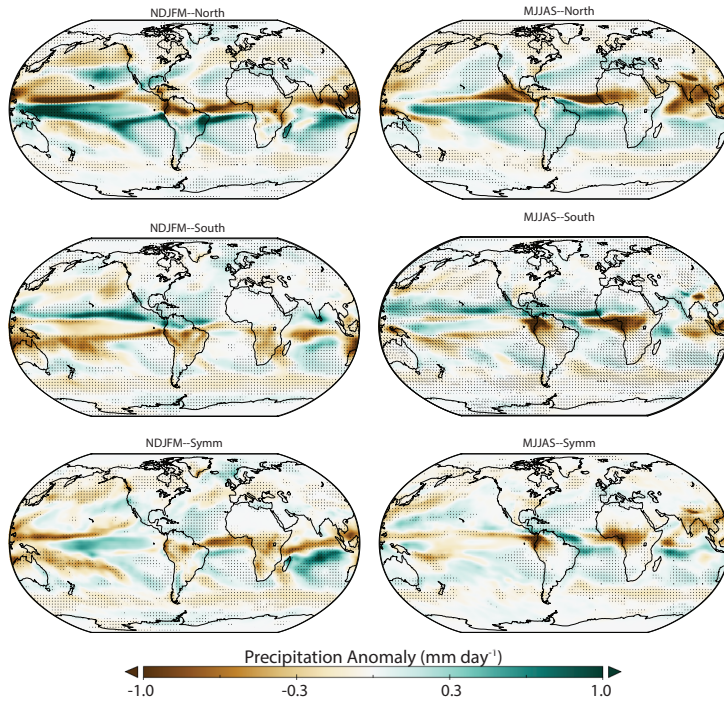
Chris Colose 7/9/2016 4:27 PM

Deleted: to

Chris Colose 7/9/2016 4:29 PM

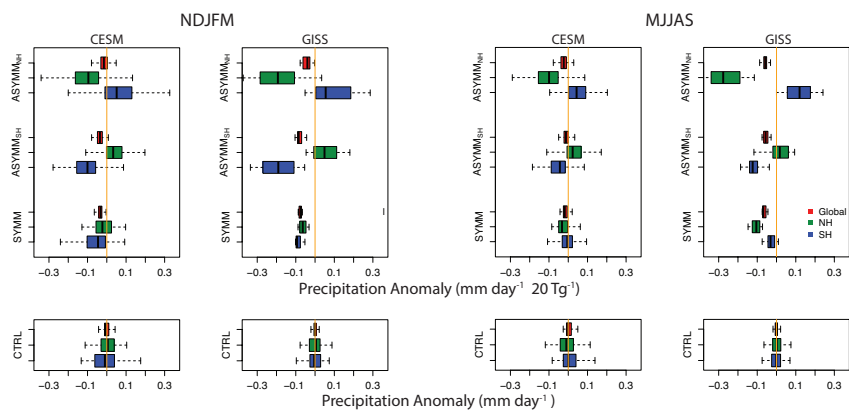
Deleted: N=the number of events used in each category, consistent with the number of listed events in Table 1 (multiplied by 15 for CESM and 3 for GISS-E2)

Precipitation (Ensemble/Event Mean)



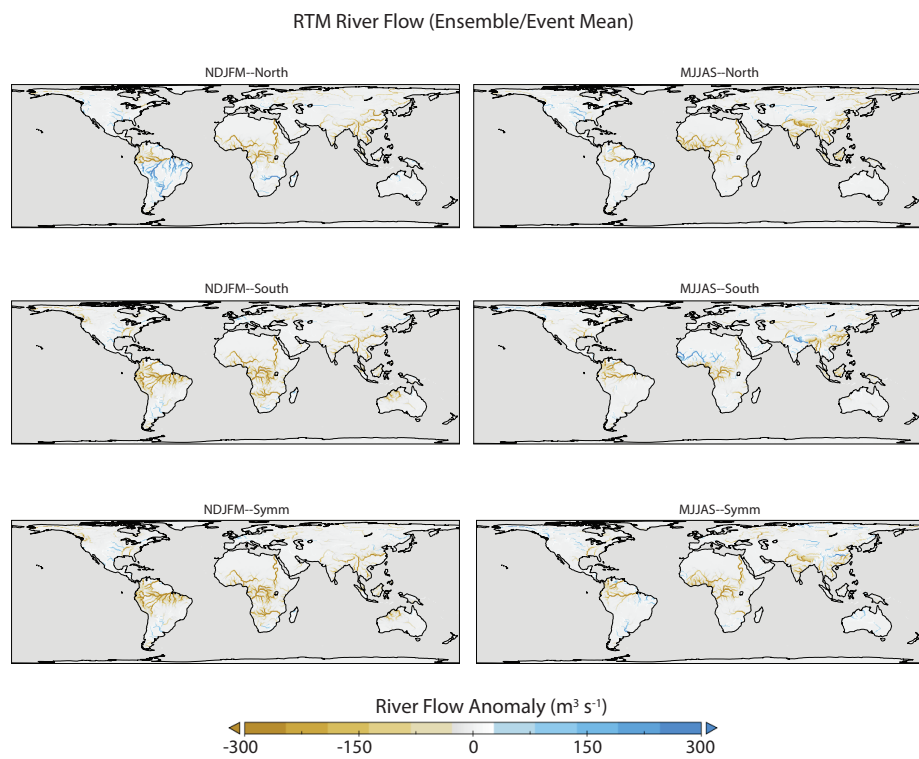
1322
1323
1324
1325
1326
1327

Figure 4. As in Figure 2, except for precipitation (mm/day).



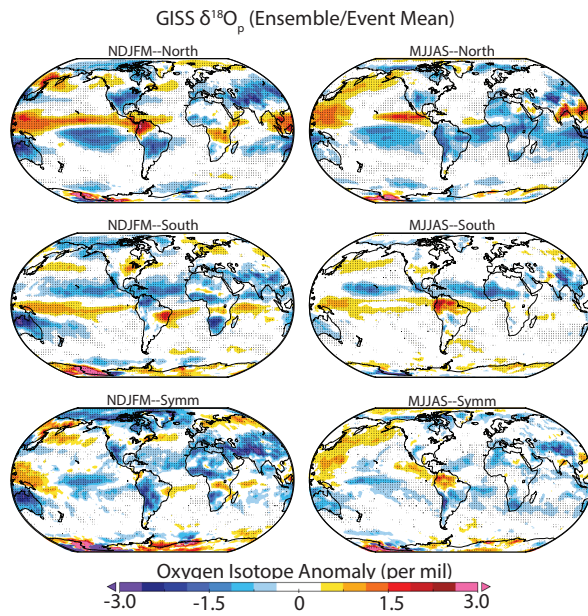
1329

1330 **Figure 5.** As in Figure 3, except for precipitation (mm/day, normalized to 20 Tg in the
 1331 forced simulations; mm/day in the control). N (not shown) is the same as in Figure 3.



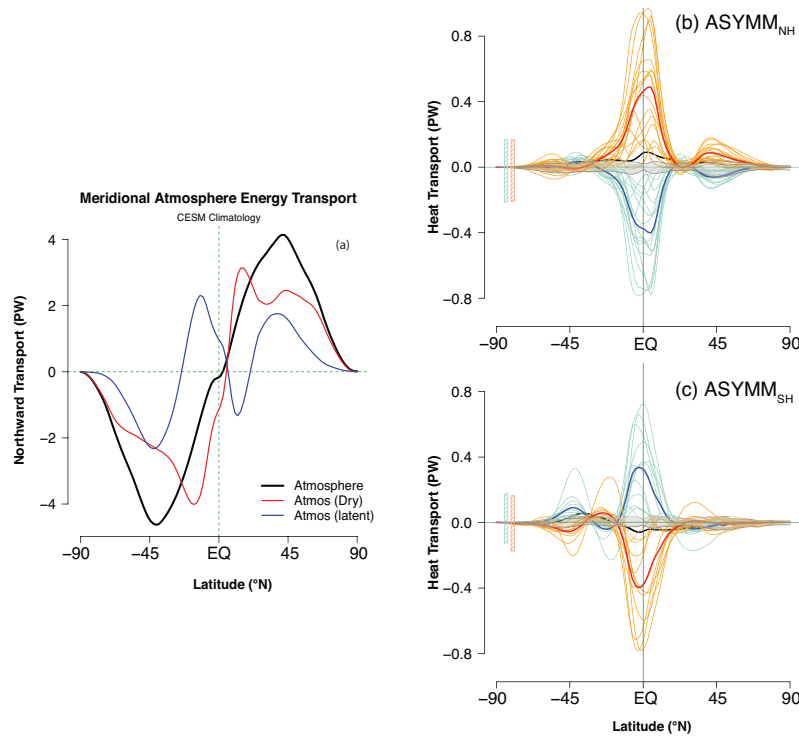
1333

1334 **Figure 6.** As in Figures 2 and 4, except for river discharge (m^3/s , or 10^{-6} Sverdrups).



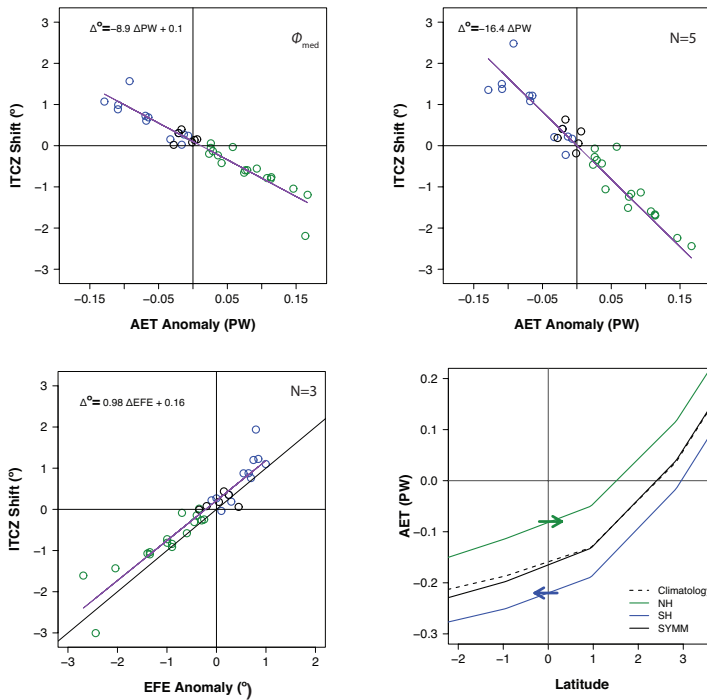
1335

1336 **Figure 7.** GISS-E2 spatial composite of the oxygen isotope anomaly (per mil) in (top
 1337 row) ASYMM_{NH₃}, (middle row) ASYMM_{SH₃}, and (bottom row) SYMM events in (left
 1338 column) NDJFM and (right column) MJJAS.



1339
 1340 **Figure 8.** a) CESM climatology of atmospheric energy transport (PW, black), dry (red),
 1341 and latent (dark blue) transports. b) Composite mean anomaly in atmospheric heat
 1342 transport for ASYMM_{NH} eruptions in total (black), dry (red), and latent (blue)
 1343 components. Lighter (orange and aqua) lines represent individual eruptions, each
 1344 averaged over 17 ensemble members. c) As in (b), except for ASYMM_{SH} eruptions. Grey
 1345 envelope corresponds to the total AET anomaly vs. latitude in a control simulation using
 1346 50 realizations of a 17-event composite (17 “events” with no external forcing
 1347 corresponding to the size of the ensemble). Vertical bars correspond to the range of
 1348 (aqua) latent and (orange) dry components of cross-equatorial energy transport (AET_{eq}) in
 1349 the control composite.

- Chris Colose 7/23/2016 7:51 PM
Deleted: e+ocean
- Chris Colose 7/23/2016 7:51 PM
Deleted: atmosphere only
- Chris Colose 7/23/2016 7:51 PM
Deleted: ocean only
- Chris Colose 7/23/2016 7:51 PM
Deleted:), moisture component of the atmosphere (latent heat, dashed aqua)
- Chris Colose 7/9/2016 5:20 PM
Deleted: Ensemble/Eruption
- Chris Colose 7/23/2016 7:52 PM
Deleted: red
- Chris Colose 7/23/2016 7:52 PM
Deleted: purple
- Chris Colose 7/23/2016 7:52 PM
Deleted: aqua
- Chris Colose 7/9/2016 5:26 PM
Deleted: Lighter lines associated with the dry and latent components indicate the eruption spread, each averaged over 14 ensemble members.
- Chris Colose 7/20/2016 4:09 PM
Deleted: composite formed
- Chris Colose 7/20/2016 4:09 PM
Deleted: from the same dates as the ASYMM_{NH} results
- Chris Colose 7/9/2016 5:27 PM
Deleted: 16



Unknown
Formatted: Font:(Default) Times New Roman

1367

1368 **Figure 9.** Annual-mean ITCZ shift represented by changes in (topleft) ϕ_{med} , and

1369 (topright) ϕ_{ITCZ} ($N = 5$) vs. change in AET_{eq} . Changes in ϕ_{ITCZ} ($N = 3$) vs. change in

1370 EFE (bottomleft). See text for definitions. Total AET vs. latitude for a small band

1371 centered around the equator for all volcanic events in (green) $ASYMM_{NH}$, (blue)

1372 $ASYMM_{SH}$, and (black) SYMM cases (bottomright). Black dashed line indicates

1373 climatological or pre-eruption AET values (different choices are indistinguishable).

1374 Colored arrows represent the direction of anomalous AET_{eq} .

Chris Colose 7/23/2016 7:19 PM
Deleted: (bottomleft)

Chris Colose 7/23/2016 7:20 PM
Deleted: (bottomright)

Table 1. List of LM Eruptions

Eruption Category	Seasons in LM Composite (MJJAS)	Seasons in LM Composite (NDJFM)
ASYMM _{NH}	870, 901, 933/934, 1081, 1176/1177, 1213/1214, 1328, 1459, 1476, 1584, 1600/1601, 1641/1642, 1719/1720, 1762/1763, 1831, 1835/1836	871, 902, 934, 1082, 1177, 1214/1215, 1329, 1460, 1585, 1601, 1641/1642, 1720, 1730, 1762/1763, 1832, 1835/1836
ASYMM _{SH}	929, 961, 1158.5/1159.5, 1232, 1268, 1275/1276, 1341/1342, 1452/1453, 1593, 1673, 1693/1694	962, 1159, 1233, 1269, 1276/1277, 1285, 1342, 1453/1454, 1674, 1694
SYMM	854, 1001, 1284/1285, 1416, 1809/1810, 1815/1816	855, 1002, 1810, 1816/1817

Chris Colose 7/19/2016 11:11 PM

Formatted: (Asian) Japanese

- 1377 1) Dates of Eruption events used in composite results, based on reconstructed stratospheric sulfate
 1378 loadings from Gao et al. (2008).
 1379 2) Combined dates with a “/” indicate a multi-season event where every inclusive month is first averaged
 1380 prior to entering the multi-eruption composite.

1381 **References**

- 1382
1383 Adam, O., Bischoff, T., and Schneider, T.: Seasonal and interannual variations of the
1384 energy flux equator and ITCZ, Part I: Zonally averaged ITCZ position, *J. Climate*, 29,
1385 [3219-3230](#), doi: [10.1175/JCLI-D-15-0512.1](#), 2016.
- 1386 [Adams, J. B., Mann, M. E., and Ammann, C. M.: Proxy evidence for an El Niño-like](#)
1387 [response to volcanic forcing, *Nature*, 426, 274–278, doi:10.1038/nature02101, 2003.](#)
- 1388 Allen, R. J., Evan, A. T., and Booth, B. B.: Interhemispheric aerosol radiative forcing and
1389 tropical precipitation shifts during the late twentieth century, *J. Climate*, 28, 8219-
1390 8246, doi:10.1175/JCLI-D-15-0148.1, 2015.
- 1391 [Anchukaitis, K. J., Buckley, B. M., Cook, E. R., Cook, B. I., D'Arrigo, R. D., and](#)
1392 [Ammann, C. M.: Influence of volcanic eruptions on the climate of the Asian monsoon](#)
1393 [region, *Geophys. Res. Lett.*, 37, L22703, doi:10.1029/2010GL044843, 2010.](#)
- 1394 Araguás-Araguás, L., Froehlich, K., and Rozanski, K.: Deuterium and oxygen-18 isotope
1395 composition of precipitation and atmospheric moisture, *Hydrol. Process.*, 14, 1341–
1396 1355, doi: [10.1002/1099-1085\(20000615\)14:8<1341::AID-HYP983>3.0.CO;2-Z](#),
1397 2000.
- 1398 Atwood, A., Wu, E., Frierson, D. M. W., Battisti, D., and Sachs, J. P.: Quantifying
1399 Climate Forcings and Feedbacks over the Last Millennium in the CMIP5–PMIP3
1400 Models, *J. Climate*, 29, 1161-1178, doi: [10.1175/JCLI-D-15-0063.1](#), 2016.
- 1401 Bischoff, T., and Schneider, T.: Energetic constraints on the position of the Intertropical
1402 Convergence Zone, *J. Climate*, 27, 4937-4951, doi:10.1175/JCLI-D-13-00650.1,
1403 2014.
- 1404 Broccoli, A. J., Dahl, K. A., and Stouffer, R. J.: Response of the ITCZ to Northern
1405 Hemisphere cooling, *Geophys. Res. Lett.*, 33, L01702, doi:10.1029/2005GL024546,

Chris Colose 7/19/2016 9:59 PM

Deleted: in press

1407 2006.

1408 Chiang, J. C. H., and Bitz, C. M.: Influence of high latitude ice cover on the marine
1409 Intertropical Convergence Zone, *Clim. Dyn.*, 25, 477– 496, doi:10.1007/s00382-005-
1410 0040-5, 2005.

1411 Chiang, J. C. H., and Friedman, A. R.: Extratropical Cooling, Interhemispheric Thermal
1412 Gradients, and Tropical Climate Change, *Ann. Rev. Earth Plan. Sci.*, 40, 383-412,
1413 doi:10.1146/annurev-earth-042711-105545, 2012.

1414 Colose, C. M., LeGrande, A. N., and Vuille, M.: The influence of volcanic eruptions on
1415 the climate of tropical South America during the last millennium in an isotope-
1416 enabled general circulation model, *Clim. Past*, 12, 961-979, doi:10.5194/cp-12-961-
1417 2016, 2016.

1418 Crowley, T. J. and Unterman, M. B.: Technical details concerning development of a
1419 1200-yr proxy index for global volcanism, *Earth Syst. Sci. Data*, 5, 187–197,
1420 doi:10.5194/essd-5-187-2013, 2013.

1421 Dansgaard, W.: Stable isotopes in precipitation, *Tellus*, 16, 436–468, doi:10.1111/j.2153-
1422 3490.1964.tb00181.x, 1964.

1423 Deser, C., Phillips, A. S., Bourdette, V., and Teng, H.: Uncertainty in climate change
1424 projections: The role of internal variability, *Clim. Dyn.*, 38, 527–546,
1425 doi:10.1007/s00382-010-0977-x, 2012.

1426 [Donohoe, A., and Battisti, D.S.: The seasonal cycle of atmospheric heating and](#)
1427 [temperature, *J. Climate*, 26, 4962-4980, doi: 10.1175/JCLI-D-12-00713.1, 2013.](#)

1428 Donohoe, A., Marshall, J., Ferreira, D., and McGee, D.: The relationship between ITCZ
1429 location and cross-equatorial atmospheric heat transport: From the seasonal cycle to

1430 the last glacial maximum, *J. Climate*, 26, 3597–3618, doi:10.1175/JCLI-D-12-
1431 00467.1, 2013.

1432 [Emile-Geay, J., Seager, R., Cane, M. A., Cook, E. R., and Haug, G. H.: Volcanoes and](#)
1433 [ENSO over the past millennium, *J. Climate*, 21, 3134–3148,](#)
1434 [doi:10.1175/2007JCLI1884.1, 2008.](#)

1435 Fasullo, J. T., and Trenberth, K. E.: The annual cycle of the energy budget. Part II:
1436 Meridional structures and poleward transports, *J. Climate*, 21, 2313–2325,
1437 doi:10.1175/2007JCLI1936.1, 2008.

1438 Friedman, A. R., Hwang, Y.-T., Chiang, J. C. H., and Frierson, D. M. W.: The
1439 interhemispheric thermal gradient over the 20th century and in future projections, *J.*
1440 *Climate*, 26, 5419–5433, doi: 10.1175/JCLI-D-12-00525.1, 2013.

1441 Frierson, D. M. W., and Hwang, Y.-T.: Extratropical influence on ITCZ shifts in slab
1442 ocean simulations of global warming, *J. Climate*, 25, 720–733, doi:10.1175/JCLI-D-
1443 11-00116.1, 2012.

1444 Frierson, D. M. W., Hwang, Y.-T., Fuckar, N. S., Seager, R., Kang, S. M., Donohoe, A.,
1445 Maroon, E. A., Liu, X., and Battisti, D. S.: Contribution of ocean overturning
1446 circulation to tropical rainfall peak in the Northern Hemisphere, *Nat. Geosci.*, 6, 940–
1447 944, doi:10.1038/ngeo1987, 2013.

1448 Gao, C., Robock, A., and Ammann, C.: Volcanic forcing of climate over the past 1500
1449 years: An improved ice core-based index for climate models, *J. Geophys. Res.*
1450 *Atmos.*, 113, D23111, doi:10.1029/2008JD010239, 2008.

1451 Haywood, J. M., Jones, A., Bellouin, N., and Stephenson, D.: Asymmetric forcing from
1452 stratospheric aerosols impacts Sahelian rainfall, *Nat. Clim. Change*, 3, 660–665,

1453 | doi:10.1038/NCLIMATE1857, 2013.

1454 | [Hoffmann, G. and Heimann, M.: Water isotope modeling in the Asian monsoon region,](#)
1455 | [Quatern. Int., 37, 115–128, doi:10.1016/1040-6182\(96\)00004-3, 1997.](#)

1456 | Hurrell, J. W., et al., The Community Earth System Model: A framework for
1457 | collaborative research, *Bull. Am. Meteorol. Soc.*, 94, 1339–1360,
1458 | doi:10.1175/BAMS-D-12-00121, 2013.

1459 | Hwang, Y.-T., and Frierson, D. M. W.: Link between the double-Intertropical
1460 | Convergence Zone problem and cloud biases over the Southern Ocean, *Proc. Natl.*
1461 | *Acad. Sci.*, 110, 4935–4940, doi:10.1073/pnas.1213302110, 2013.

1462 | Hwang, Y.-T., Frierson, D. M. W., and Kang, S. M.: Anthropogenic sulfate aerosol and
1463 | the southward shift of tropical precipitation in the 20th century, *Geophys. Res. Lett.*,
1464 | 40, 1-6, doi: 10.1002/grl50502, 2013.

1465 | Iles, C. E., Hegerl, G. C., Schurer, A. P., and Zhang, X.: The effect of volcanic eruptions
1466 | on global precipitation, *J. Geophys. Res. Atmos.*, 118, 8770–8786,
1467 | doi:10.1002/jgrd.50678, 2013.

1468 | Iles, C. E., and Hegerl, G. C., The global precipitation response to volcanic eruptions in
1469 | the CMIP5 models, *Environ. Res. Lett.*, 9, 104012, doi:10.1088/1748-
1470 | 9326/9/10/104012, 2014.

1471 | [Iles, C. E., and Hegerl, G.C., Systematic change in global patterns of streamflow](#)
1472 | [following volcanic eruptions, *Nat. Geosci.*, 8, 838-842, doi:10.1038/ngeo2545, 2015.](#)

1473 | Kang, S. M., Held, I. M., Frierson, D. M. W., and Zhao, M.: The response of the ITCZ to
1474 | extratropical thermal forcing: Idealized slab ocean experiments with a GCM, *J.*
1475 | *Climate*, 21, 3521–3532, doi:10.1175/2007JCLI2146.1, 2008.

1476 Kang, S. M., Frierson, D. M. W., and Held, I. M.: The tropical response to extratropical
1477 thermal forcing in an idealized GCM: The importance of radiative feedbacks and
1478 convective parameterization, *J. Atmos. Sci.*, 66, 2812–2827,
1479 doi:10.1175/2009JAS2924.1, 2009.

1480 Kang, S. M., Seager, R., Frierson, D. M. W., and Liu, X.: Croll revisited: Why is the
1481 northern hemisphere warmer than the southern hemisphere?, *Clim. Dyn.*, 44, 1457–
1482 1472, doi:10.1007/s00382-014-2147-z, 2014.

1483 Kravitz, B., and Robock, A.: Climate effects of high-latitude volcanic eruptions: Role of
1484 the time of year, *J. Geophys. Res.*, 116, D01105, doi:10.1029/2010JD014448, 2011.

1485 Lacis, A., Hansen, J. and Sato, M.: Climate forcing by stratospheric aerosols, *Geophys.*
1486 *Res. Lett.*, 19, 1607-1610, doi:10.1029/92GL01620, 1992.

1487 Lacis, A.: Volcanic aerosol radiative properties, *PAGES Newsletter*, 23, 2, 50-51, 2015.

1488 LeGrande, A.N., and Schmidt, G.A.: Ensemble, water-isotope enabled, coupled general
1489 circulation modeling insights into the 8.2-kyr event, *Paleoceanogr.*, 23, PA3207,
1490 doi:10.1029/2008PA001610, 2008.

1491 LeGrande, A.N., and Schmidt, G.A.: Sources of Holocene variability of oxygen isotopes
1492 in paleoclimate archives, *Clim. Past*, 5, 441-455, doi:10.5194/cp-5-441-2009, 2009.

1493 LeGrande, A.N., and Anchukaitis, K. J.: Volcanic eruptions and climate, *PAGES*
1494 *Newsletter*, 23, 2, 46-47, 2015.

1495 Liu, F., Chai, J., Wang, B., Liu, J., Zhang, X., Wang, Z.: Global monsoon precipitation
1496 responses to large volcanic eruptions, *Sci. Rep.*, 6, 24331, doi: 10.1038/srep24331,
1497 | 2016.

1498 | [Mann, M. E., Cane, M. A., Zebiak, S. E. and Clement, A.: Volcanic and solar forcing of](#)
1499 | [the tropical Pacific over the past 1000 years, J. Climate, 18, 447–456,](#)
1500 | [doi:10.1175/JCLI-3276.1, 2005.](#)

1501 | Mann, G., Dhomse, S., Deshler, T., Timmreck, C., Schmidt, A., Neely, R., and
1502 | Thomason, L.: Evolving particle size is the key to improved volcanic forcings,
1503 | PAGES Newsletter., 23, 2, 52-53, 2015.

1504 | Maroon, E. A., Frierson, D. M. W., Kang, S. M., and Scheff, J.: The precipitation
1505 | response to an idealized subtropical continent, J. Climate, [29, 4543-4564,](#)
1506 | [doi:10.1175/JCLI-D-15-0616.1, 2016,](#)

1507 | Marshall, J., Donohoe, A., Ferreira, D., and McGee, D.: The ocean’s role in setting the
1508 | mean position of the Intertropical Convergence Zone, Clim. Dyn., 42, 1967–1979,
1509 | doi:10.1007/s00382-013-1767-z, 2013.

1510 | McGee, D., A. Donohoe, J. Marshall, D. Ferreira , Changes in ITCZ location and cross-
1511 | equatorial heat transport at the Last Glacial Maximum, Heinrich Stadial 1, and the
1512 | mid-Holocene, Earth Plan. Sci. Lett., 390, 69-79, doi:10.1016/j.epsl.2013.12.043,
1513 | 2014.

1514 | Miller, R.L., et al., CMIP5 historical simulations (1850-2012) with GISS-E2 ModelE2. J.
1515 | Adv. Model. Earth Syst., 6(2), 441-477, doi:10.1002/2013MS000266, 2014.

1516 | Neelin, J. D. and Held, M.: Modeling tropical convergence based on the moist static
1517 | energy budget, Mon. Wea. Rev., 115, 3-12, doi: 10.1175/1520-
1518 | 0493(1987)115<0003:MTCBOT>2.0.CO;2, 1987.

1519 | Oleson, K. W., et al., Technical description of version 4.0 of the Community Land Model
1520 | (CLM), NCAR Tech. Note NCAR/TN-478+STR, 257 pp., Natl. Cent. for Atmos.

Chris Colose 7/10/2016 5:18 PM
Deleted: , in press.

1522 Res., Boulder, Colo, 2010.

1523 Oman, L., Robock, A., Stenchikov, G., Schmidt, G. A., and Ruedy, R.: Climatic response
1524 to high latitude volcanic eruptions, *J. Geophys. Res.*, 110, D13103,
1525 doi:10.1029/2004JD005487, 2005.

1526 Oman, L., Robock, A., Stenchikov, G. L., and Thordarson, T.: High-latitude eruptions
1527 cast shadow over the African monsoon and the flow of the Nile, *Geophys. Res. Lett.*,
1528 33, L18711, doi:10.1029/2006GL027665, 2006.

1529 Ortega, P., Lehner, F., Swingedouw, D., Masson-Delmotte, V., Raible, C. C., Casado,
1530 M., and Yiou, P.: A model-tested North Atlantic Oscillation reconstruction for the
1531 past millennium, *Nature*, 523, 71–74, doi:10.1038/nature14518, 2015.

1532 Otto-Bliesner, B. L., Brady, E. C., Fasullo, J., Jahn, A., Landrum, L., Stevenson, S.,
1533 Rosenbloom, N., Mai, A., and Strand, G.: Climate Variability and Change since 850
1534 C.E, Climate variability and change since 850 C.E.: An ensemble approach with the
1535 Community Earth System Model (CESM), *Bull. Am. Meteorol. Soc.*, [97, 735-754](#),
1536 doi:10.1175/BAMS-D-14-00233.1, 2016.

1537 Oueslati, B., and Bellon, G., The double ITCZ bias in CMIP5 models: interaction
1538 between SST, large-scale circulation and precipitation, *Clim. Dyn.*, 44, 585-607,
1539 doi:10.1007/s00382-015-2468-6, 2015.

1540 Pausata, F. S. R., Chafik, L., Caballero, R., and Battisti, D. S.: Impacts of a high-latitude
1541 volcanic eruption on AMOC and ENSO, *Proc. Nat. Acad. Sci.*, 112, 13784-13788,
1542 doi: 10.1073/pnas.1509153112, 2015.

1543 Ridley, H. E., et al., Aerosol forcing of the position of the intertropical convergence zone
1544 since AD 1550, *Nat. Geosci.*, 8, 195-200, doi:10.1038/ngeo2353, 2015.

Chris Colose 7/17/2016 9:19 PM

Deleted: , in press

1546 Robock, A. and Mao, J.: Winter warming from large volcanic eruptions, *Geophys. Res.*
1547 *Lett.*, 19, 2405-2408, doi:10.1029/92GL02627, 1992.

1548 Robock, A. and Mao, J.: The volcanic signal in surface temperature observations. *J.*
1549 *Climate*, 8, 1086-1103, doi:10.1175/1520-0442(1995)008<1086:TVSIST>2.0.CO;2,
1550 1995.

1551 Robock, A., Volcanic eruptions and climate, *Rev. Geophys.*, 38, 191–219,
1552 doi:10.1029/1998RG000054, 2000.

1553 Sato, M., Hansen, J. E., McCormick, M. P., and Pollack, J. B.: Stratospheric aerosol
1554 optical depths, 1850-1990, *J. Geophys. Res.*, 98, 22987-22994,
1555 doi:10.1029/93JD02553, 1993.

1556 Schmidt, G. A., Hoffmann, G., Shindell, D. T., and Hu, Y.: Modeling atmospheric stable
1557 water isotopes and the potential for constraining cloud processes and stratosphere-
1558 troposphere water exchange, *J. Geophys. Res.*, 110, D21314,
1559 doi:10.1029/2005JD005790, 2005.

1560 Schmidt, G. A., LeGrande, A. N., and Hoffmann, G.: Water isotope expressions of
1561 intrinsic and forced variability in a coupled ocean-atmosphere model, *J. Geophys.*
1562 *Res.*, 112, D10103, doi:10.1029/2006JD007781, 2007.

1563 Schmidt, G.A., et al., , Climate forcing reconstructions for use in PMIP simulations of the
1564 last millennium (v1.0), *Geosci. Model Dev.*, 4, 33-45, doi:10.5194/gmd-4-33-2011,
1565 2011.

1566 Schneider, T., Bischoff, T., and Haug, G. H.: Migrations and dynamics of the
1567 Intertropical Convergence Zone, *Nature*, 513, 45–53, doi:10.1038/nature13636, 2014.

1568 Shindell, D. T., Schmidt, G. A., Mann, M. E., and Faluvegi, G.: Dynamic winter climate

1569 response to large tropical volcanic eruptions since 1600, *J. Geophys. Res.*, 109,
 1570 D05104, doi:10.1029/2003JD004151, 2004.

1571 Sigl, M., et al. , Timing and climate forcing of volcanic eruptions for the past 2,500 years,
 1572 *Nature*, 523, 543-549, doi:10.1038/nature14565, 2015.

1573 Stenchikov, G., Robock, A., Ramaswamy, V., Schwarzkopf, M. D., Hamilton, K., and
 1574 Ramachandran, S.: Arctic Oscillation response to the 1991 Mount Pinatubo eruption,
 1575 Effects of volcanic aerosols and ozone depletion, *J. Geophys. Res.*, 107, 4803,
 1576 doi:10.1029/2002JD002090, 2002.

1577 [Stevenson, S., Otto-Bliesner, B., Fasullo, J., and Brady, E.: “El Niño Like” hydroclimate](#)
 1578 [responses to last millennium volcanic eruptions, *J. Climate*, 29, 2907-2921,](#)
 1579 [doi:10.1175/JCLI-D-15-0239.1, 2016.](#)

1580 Stothers, R. B.: The Great Tambora Eruption in 1815 and its aftermath, *Science*, 224,
 1581 1191–1198, doi:10.1126/science.224.4654.1191, 1984.

1582 [Trenberth, K. E.: Using atmospheric budgets as a constraint on surface fluxes, *J. Climate*,](#)
 1583 [10, 2796–2809, doi:10.1175/1520-0442\(1997\)010<2796:UABAAC>2.0.CO;2, 1997.](#)

1584 Trenberth, K. E., and Dai, A.: Effects of Mount Pinatubo volcanic eruption on the
 1585 hydrological cycle as an analog of geoengineering, *Geophys. Res. Lett.*, 34, L15702,
 1586 doi:10.1029/2007GL030524, 2007.

1587 Trenberth, K. E., and Caron, J. M.: Estimates of meridional atmosphere and ocean heat
 1588 transports, *J. Climate*, 14, 3433-3443, doi:10.1175/1520-
 1589 0442(2001)014<3433:EOMAAO>2.0.CO;2, 2001.

1590 Vuille, M., Bradley, R. S., Werner, M., Healy, R., and Keimig, F.: Modeling d¹⁸O in
 1591 precipitation over the tropical Americas: 1. Interannual variability and climatic

Mathias Vuille 7/21/2016 11:41 AM
 Deleted: H

Mathias Vuille 7/21/2016 11:41 AM
 Deleted: R

Mathias Vuille 7/21/2016 11:41 AM
 Deleted: L

Mathias Vuille 7/21/2016 11:41 AM
 Deleted: M

Mathias Vuille 7/21/2016 11:41 AM
 Deleted: V

Mathias Vuille 7/21/2016 11:41 AM
 Deleted: E

1598 controls, *J. Geophys. Res.*, 108, D6, 4174, doi:10.1029/2001JD002038, 2003.

1599 Wunsch, C., The total meridional heat flux and its oceanic and atmospheric partition, *J.*
1600 *Climate*, 18, 4374–4380, doi:10.1175/JCLI3539.1, 2005.

1601 Yoshimori, M., and Broccoli, A. J.: Equilibrium response of an atmosphere-mixed layer
1602 | ocean model to different radiative forcing agents: Global and zonal mean response, *J.*
1603 *Climate*, 21, 4399-4423, doi:10.1175/2008jcli2172.1, 2008.

1604 Yoshimori, M., and Broccoli, A. J.: On the link between Hadley circulation changes and
1605 radiative feedback processes, *Geophys. Res. Lett.*, 36, L20703,
1606 doi:10.1029/2009GL040488, 2009.

1607

1608

1609 |

Chris Colose 7/23/2016 7:23 PM
Deleted: 288

1611 **Supplemental Figure Captions**

1612

1613 **Figure S1.** Zonal-mean temperature anomalies as a function of atmospheric pressure and

1614 latitude in CESM volcanic eruption composites for [each](#) event and season classifications

1615 [discussed in text](#).

1616 **Figure S2.** GISS spatial composite of temperature anomaly ($^{\circ}\text{C}$) for (top row)

1617 ASYMM_{NH} , (middle row) ASYMM_{SH} , and (bottom row) SYMM events, each in (left

1618 column) NDJFM and (right column) MJJAS. Note that scaling of colorbar is different

1619 from CESM composite (Figure 2).

1620 **Figure S3.** As in Figure S2, except for precipitation (mm/day). Note colorbar range

1621 difference compared to CESM composite (Figure 4).

1622 **Figure S4.** Precipitation anomaly (mm/day) for the 1763 C.E. Laki eruption for NDJFM.

1623 Results displayed for all [18](#) ensemble members in CESM relative to the 1757-1761 C.E.

1624 NDJFM mean. Surface air temperature anomalies ($^{\circ}\text{C}$) averaged over the Niño 3.4 region

1625 displayed at topright of each panel. Note colorbar range difference compared to CESM

1626 all-event composite (Figure 4).

1627 **Figure S5.** Precipitation asymmetry index (unitless) as defined in text vs. NH minus SH

1628 AOD gradient (hemispheric sulfate loadings divided by 75 Tg for the CESM results).

1629 Results displayed for both seasons in LM time series. Since most of the LM time series

1630 features zero or low volcanic activity, all seasons where $-0.1 < \text{AOD gradient} < 0.1$ are

1631 shown by dashed box and whisker (GISS) and solid box only (CESM). The whisker

1632 lengths are very similar between the two models, and were omitted to avoid visual

1633 overlap. Results presented for the [18](#) and 3-member ensemble mean for each season,

1634 which suppresses the variability (represented by the box and whisker spread) for the non-

Chris Colose 7/18/2016 1:49 PM
Deleted: as

Chris Colose 7/17/2016 11:29 PM
Deleted: 15

Chris Colose 7/23/2016 8:24 PM
Deleted: -

Chris Colose 7/17/2016 11:30 PM
Deleted: 15

1639 eruption compilation but allows for comparison with the ensemble-mean volcanic
1640 responses.

1641 **Figure S6.** Niño 3.4 SST anomalies for all ASYMM_{NH} events, centered on Year 0 (the
1642 January before each eruption). The mean SST anomaly averaged over all eruption and
1643 ensemble members is shown as red line, and the eruption spread is shown as gray shading
1644 (after averaging [18](#) ensemble members). Composite-mean NH aerosol loading (Tg),
1645 aligned in the same way, is shown as purple line.

1646 **Figure S7.** Composite Sea Surface Height (cm) and surface wind anomalies for
1647 ASYMM_{NH} events. Composite formed from the boreal winter events in Table 1 in main
1648 text. [Blue box shows the Niño 3.4 region.](#)

1649
1650 **Figure S8.** [Distribution of precipitation anomalies \(mm/day\) in CESM \(top\) and GISS-](#)
1651 [E2 \(bottom\) during MJJAS averaged broadly over the Asian-Pacific monsoon sector](#)
1652 [\(65°-150°E, 10°-40°N\), including regions of the Indian summer monsoon, western North](#)
1653 [Pacific summer monsoon, and the East Asian summer monsoon. Each eruption is taken to](#)
1654 [be an independent event, and there are more events in CESM due to the greater ensemble](#)
1655 [size \(note difference in y-axis scale and slightly different bin width\). Solid lines](#)
1656 [correspond to a normal distribution for the \(red, ASYMM_{NH}; blue, ASYMM_{SH}; black,](#)
1657 [SYMM\) events.](#)

1658
1659 **Figure S9.** Animation from May of Year -2 to December of Year +6 (as discussed in
1660 text) of monthly temperature anomalies (°C) associated with ASYMM_{NH} volcanic forcing
1661 in CESM. For each time step, the global aerosol loading (in Tg) and hemispheric

Chris Colose 7/17/2016 11:29 PM
Deleted: 15

Chris Colose 7/19/2016 11:56 PM
Deleted: S8

1664 difference in loading (NH minus SH) are displayed. Months exceeding the 8 Tg global
1665 aerosol loading in the G08 dataset are displayed in red.

1666 | **Figure S10.** As in Figure S9, except for $ASYMM_{SH}$.

1667 | **Figure S11.** As in Figure S9, except for precipitation (mm/day).

1669 | **Figure S12.** As in Figure S11, except for $ASYMM_{SH}$.

1671
1672

1673

1674

Chris Colose 7/19/2016 11:56 PM

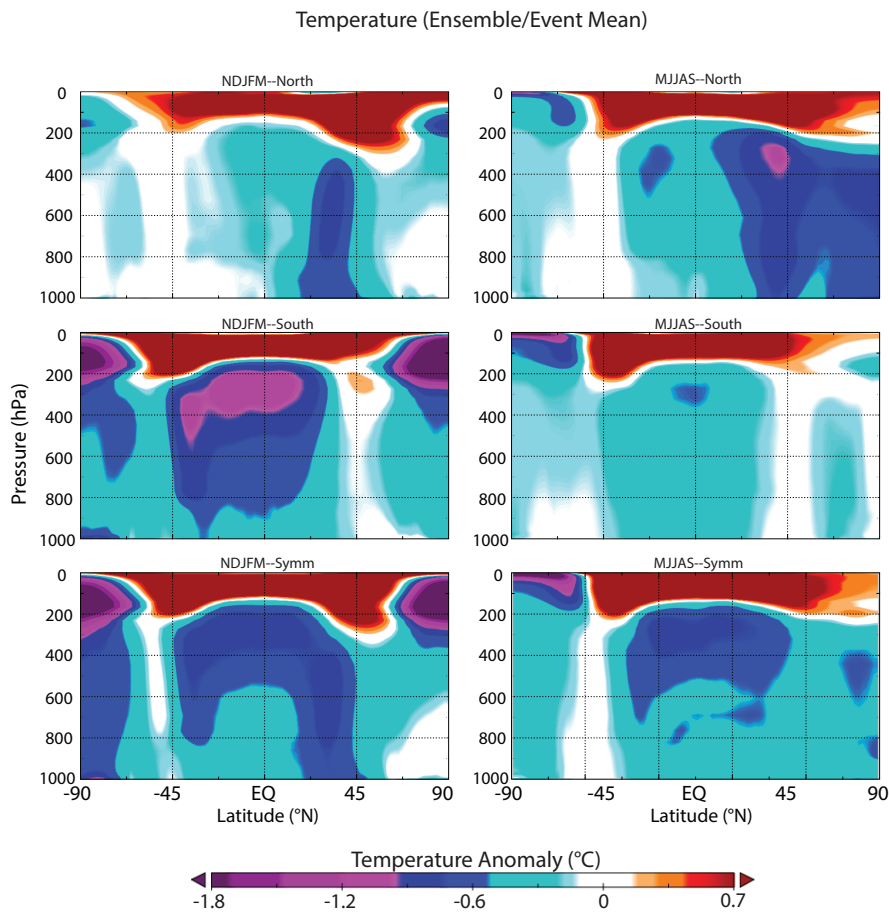
Deleted: S9

Chris Colose 7/19/2016 11:56 PM

Deleted: S10

Chris Colose 7/19/2016 11:56 PM

Deleted: S11



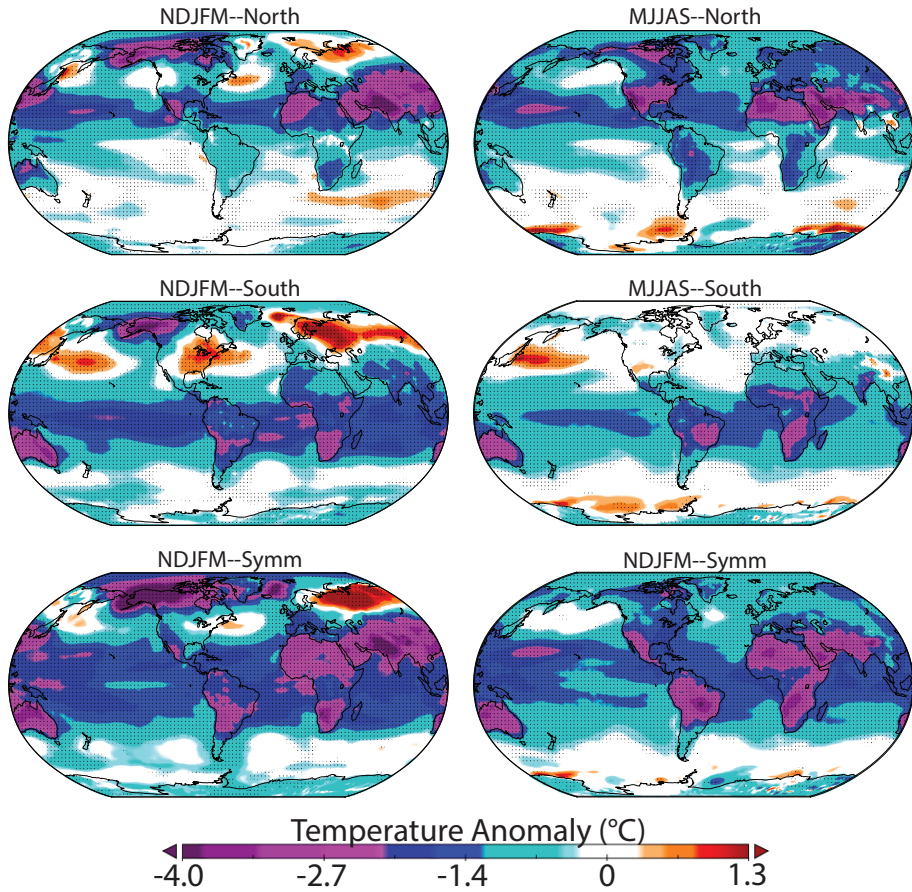
1675

1679 **Figure S1.** Zonal-mean temperature anomalies as a function of atmospheric pressure and
1680 latitude in CESM volcanic eruption composites [for each event and season classifications](#)
1681 [discussed in text](#)

1682
1683
1684
1685
1686
1687
1688
1689
1690
1691
1692
1693

Chris Colose 7/18/2016 1:49 PM
Deleted: for event and season classifications
as discussed in text

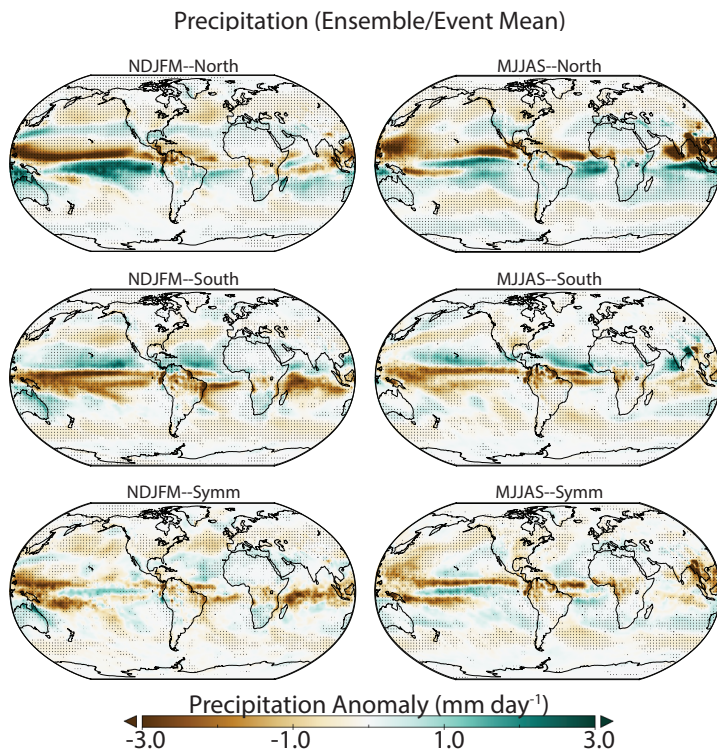
Temperature (GISS Ensemble/Event Mean)



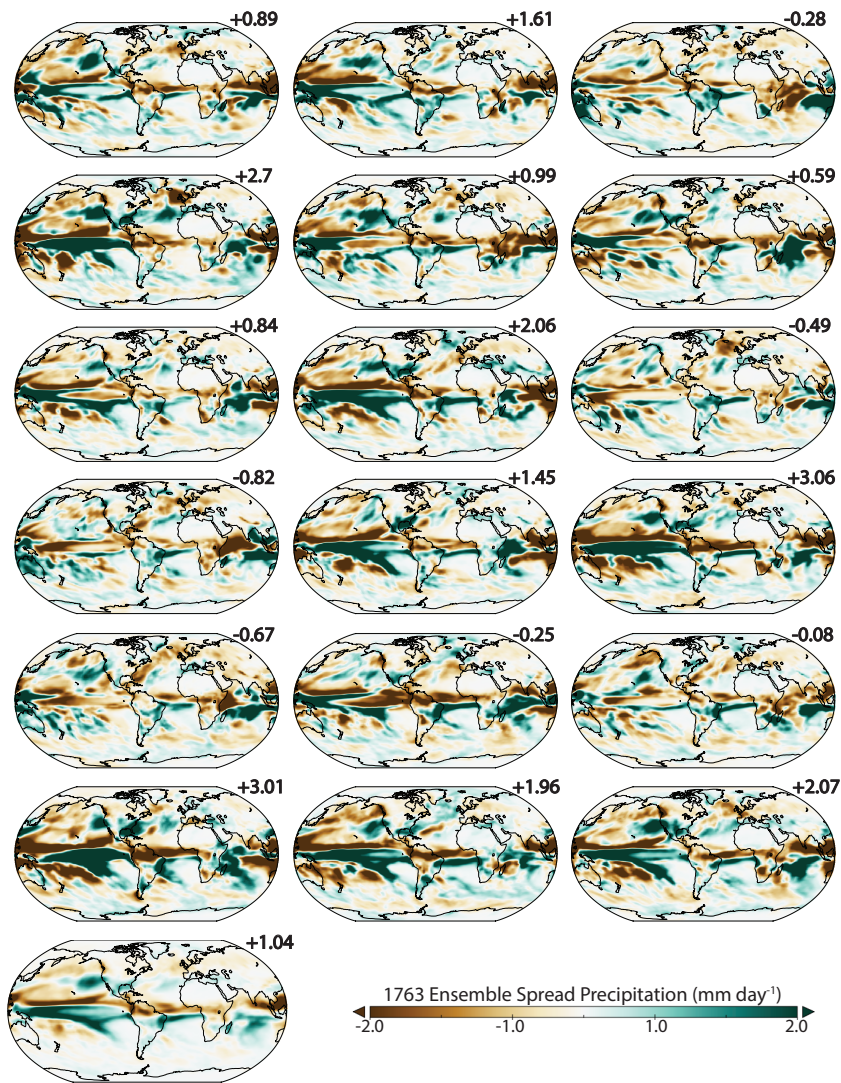
1696
1697

Figure S2. GISS spatial composite of temperature anomaly ($^{\circ}\text{C}$) for (top row)

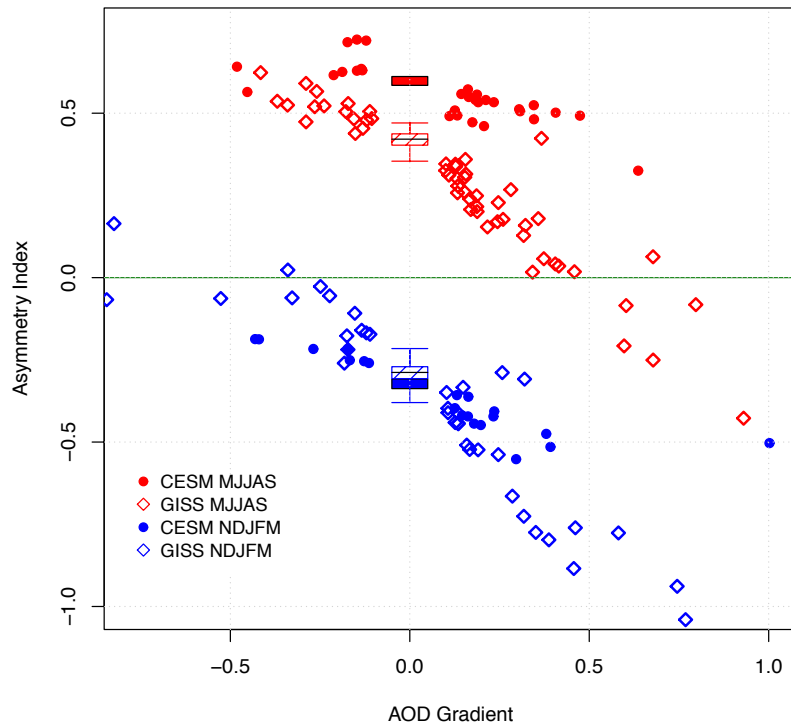
1698 ASYMM_{NH}, (middle row) ASYMM_{SH}, and (bottom row) SYMM events, each in (left
1699 column) NDJFM and (right column) MJJAS. Note that scaling of colorbar is different
1700 from CESM composite (Figure 2).



1701
 1702 **Figure S3.** As in Figure S2, except for precipitation (mm/day). Note colorbar range
 1703 difference compared to CESM composite (Figure 4).
 1704



1705
 1706 **Figure S4.** Precipitation anomaly (mm/day) for the 1763 C.E. Laki eruption for NDJFM.
 1707 Results displayed for all 18 ensemble members in CESM relative to the 1757-1761 C.E.
 1708 NDJFM mean. Surface air temperature anomalies ($^{\circ}\text{C}$) averaged over the Niño 3.4 region
 1709 displayed at topright of each panel. Note colorbar range difference compared to CESM
 1710 all-event composite (Figure 4).



1711 **Figure S5.** Precipitation asymmetry index (unitless) as defined in text vs. NH minus SH
 1712 AOD gradient (hemispheric sulfate loadings divided by 75 Tg for the CISM results).
 1713 Results displayed for both seasons in LM time series. Since most of the LM time series
 1714 features zero or low volcanic activity, all seasons where $-0.1 < \text{AOD gradient} < 0.1$ are
 1715 shown by dashed box and whisker (GISS) and solid box only (CISM). The whisker
 1716 lengths are very similar between the two models, and were omitted to avoid visual
 1717 overlap. Results presented for the 18 and 3-member ensemble mean for each season,
 1718 which suppresses the variability (represented by the box and whisker spread) for the non-
 1719 eruption compilation but allows for comparison with the ensemble-mean volcanic
 1720 responses.
 1721 responses.

Chris Colose 7/23/2016 8:24 PM
 Deleted: -

Chris Colose 7/17/2016 11:29 PM
 Deleted: 15

1724 CESM LME uses the Parallel Ocean Program (POP2; Smith et al. 2010) as the
1725 ocean model component. This is where the sea surface temperature (SST) and sea surface
1726 height (SSH) diagnostics presented in Figure S6 and S7 are calculated. The model
1727 features 384 (latitude) x 320 (longitude) ocean grid points, with variable horizontal
1728 resolution that increases toward the tropics. There are 60 vertical levels, gradually
1729 increasing from 10 m resolution in the top 150 m to ~250 m below 3 km depth.

1730 To perform a superposed epoch analysis for the state of the Pacific following all
1731 ASYMM_{NH} events, the Niño 3.4 index is calculated for each ensemble member in CESM
1732 (averaging the SST from 120°W-170°W, 5°S-5°N) with the long-term annual cycle
1733 removed. “Year 0” corresponds to the January before each eruption. We only show
1734 results for ASYMM_{NH}, since no distinguishable behavior in the Niño 3.4 time series is
1735 exhibited for the other eruption classifications, as discussed in text. Months before Year 0
1736 may feature a non-zero aerosol loading (as in Figure S6) due to the 8 Tg threshold for
1737 defining an eruption not being satisfied, or due to overlap with previous eruptions. Unlike
1738 the spatial composites discussed in the main text, pre-eruption months presented below
1739 are not replaced with the pre-eruption dates of previous overlapping eruptions. However,
1740 in the composite-mean, the aerosol loading is negligible for pre-eruption years, as well as
1741 after ~5 years after the composite eruption, and does not bias the results.

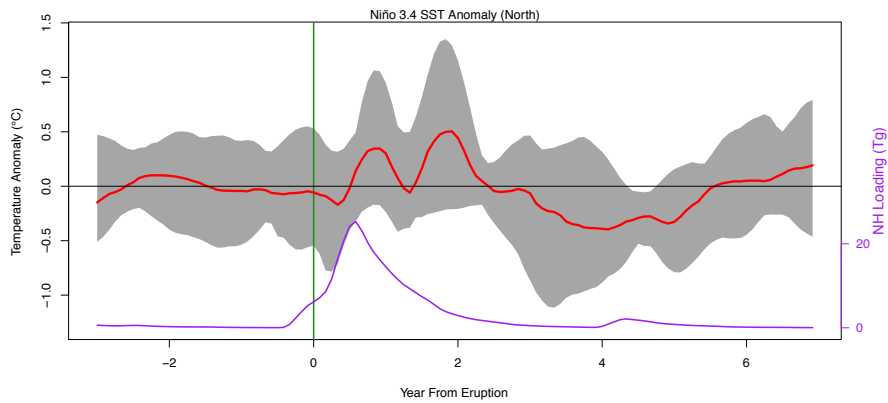
1742 Figure S6 presents the Niño 3.4 time series averaged over all ASYMM_{NH}
1743 eruptions and ensemble members. Grey shading corresponds to the eruption spread after
1744 averaging over the ensemble members. Since the CESM ENSO amplitude is large, even
1745 after averaging over 18 members, the pre-eruption envelope is still quite wide (individual

Chris Colose 7/23/2016 8:24 PM
Deleted: -

Chris Colose 7/23/2016 8:24 PM
Deleted: -

Chris Colose 7/17/2016 11:22 PM
Deleted: 15

1749 events may be on the order of 5°C above normal). Averaging over fewer ensemble
1750 members would progressively increase the width of the envelope.
1751
1752
1753
1754
1755

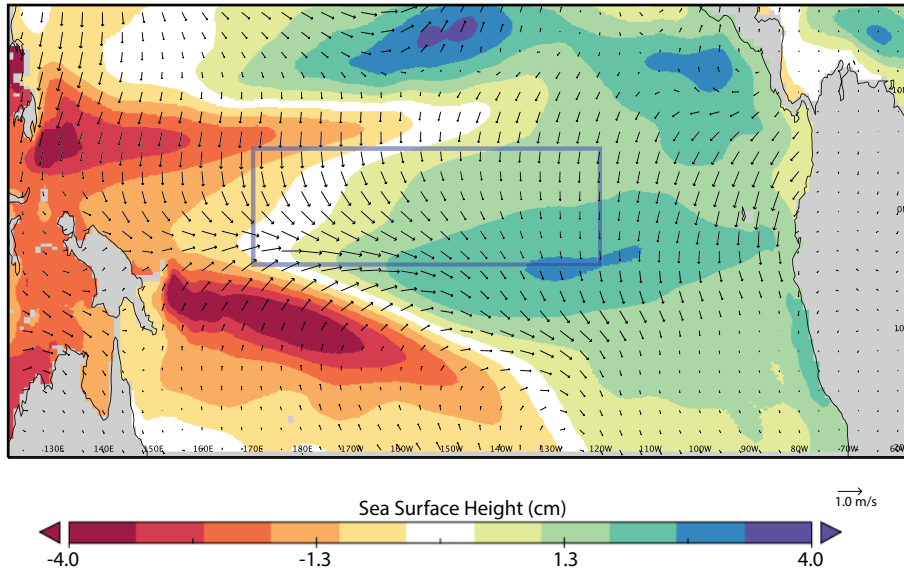


1756
1757 **Figure S6.** Niño 3.4 SST anomalies for all ASYMM_{NH} events, centered on Year 0 (the
1758 January before each eruption). The mean SST anomaly averaged over all eruption and
1759 ensemble members is shown as red line, and the eruption spread is shown as gray shading
1760 (after averaging 18 ensemble members). Composite-mean NH aerosol loading (Tg),
1761 aligned in the same way, is shown as purple line.

1762
1763
1764
1765
1766
1767

Chris Colose 7/17/2016 11:22 PM
Deleted: 15

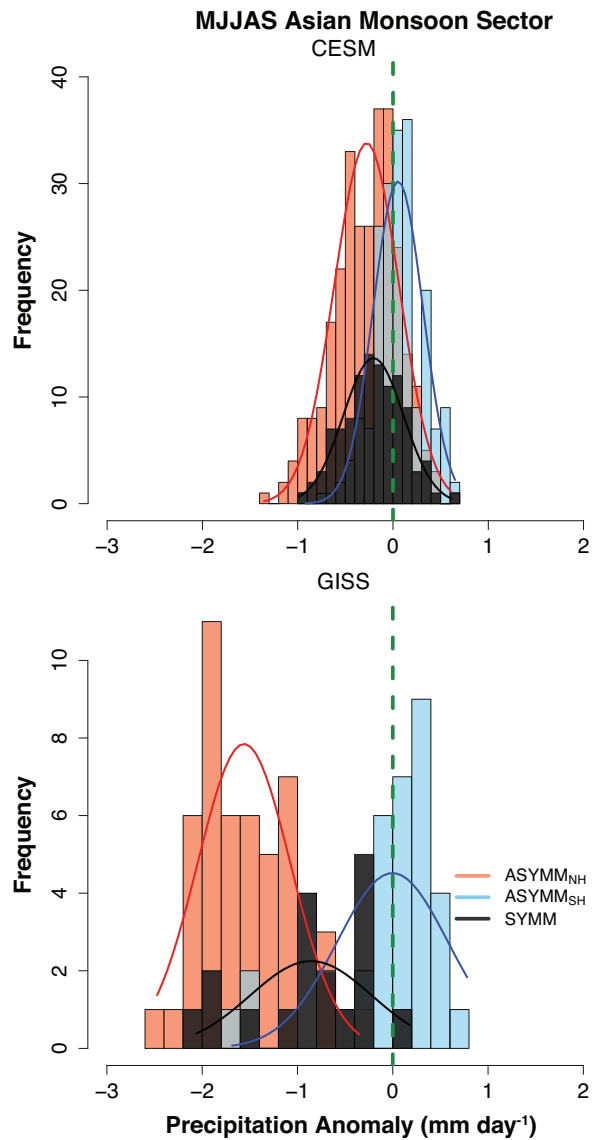
Sea Surface Height and Surface Wind Anomalies (North)



1769
1770 **Figure S7.** Composite Sea Surface Height (cm) and surface wind anomalies for
1771 ASYMM_{NH} events. Composite formed from the boreal winter events in Table 1 in main
1772 text. [Blue box shows the Niño 3.4 region.](#)

1773
1774
1775

Chris Colose 7/17/2016 11:18 PM
Deleted: . Blue box shows the Niño 3.4 region



Unknown
Formatted: Font:(Default) Times New Roman

1778
1779
1780
1781
1782
1783
1784
1785
1786

Figure S8. Distribution of precipitation anomalies (mm/day) in CESM (top) and GISS-E2 (bottom) during MJJAS averaged broadly over the Asian-Pacific monsoon sector (65°-150°E, 10°-40°N), including regions of the Indian summer monsoon, western North Pacific summer monsoon, and the East Asian summer monsoon. Each eruption is taken to be an independent event, and there are more events in CESM due to the greater ensemble size (note difference in y-axis scale and slightly different bin width). Solid lines correspond to a normal distribution for the (red, ASYMM_{NH}; blue, ASYMM_{SH}; black, SYMM) events.

1788 In the animations below, monthly temperature and precipitation anomalies from
 1789 CESM (for each event, using five years as a pre-eruption reference period) are shown in a
 1790 loop from May of Year -2 to December of Year +6, where year 0 and month 1
 1791 corresponds to the January before each eruption, defined based on the same criteria as in
 1792 main text. The animation shows the average anomaly field for all eruptions among [18](#)
 1793 ensemble members, which suppresses the internal variability in pre-eruption months.
 1794 There is still variability in the sequence of pre-eruption composites due to the finite
 1795 number of realizations of natural variability, non-zero aerosol loading (only when the 8
 1796 Tg global aerosol loading is exceeded is an event aligned with Year 0), overlap with
 1797 previous eruptions, in addition to non-volcanic radiative forcings that are still present in
 1798 [13/18](#) of the ensemble members.

1799 <https://av.tib.eu/media/18569?48>,
 1800 **Figure S9.** Animation from May of Year -2 to December of Year +6 (as discussed in
 1801 text) of monthly temperature anomalies (°C) associated with ASYMM_{NH} volcanic forcing
 1802 in CESM. For each time step, the global aerosol loading (in Tg) and hemispheric
 1803 difference in loading (NH minus SH) are displayed. Months exceeding the 8 Tg global
 1804 aerosol loading in the G08 dataset are displayed in red.
 1805

1806 <https://av.tib.eu/media/18571?16>
 1807 **Figure S10.** As in Figure S9, except for ASYMM_{SH}.

1808 <https://av.tib.eu/media/18570?32>
 1809 **Figure S11.** As in Figure S9, except for precipitation (mm/day).

1810 <https://av.tib.eu/media/18572?0>
 1811 **Figure S12.** As in Figure S11, except for ASYMM_{SH}.

1812
 1813
 1814
 1815
 1816
 1817

Chris Colose 7/17/2016 11:29 PM
 Deleted: 15

Chris Colose 7/17/2016 11:29 PM
 Deleted: 10

Chris Colose 7/17/2016 11:29 PM
 Deleted: 15

Chris Colose 7/23/2016 8:34 PM
 Deleted: https://www.dropbox.com/s/2xzvo0sxb8rj9p3/VOLCN_T_v2.flv?dl=0

Chris Colose 7/19/2016 8:32 PM
 Deleted: S8

Chris Colose 7/23/2016 8:33 PM
 Deleted: https://www.dropbox.com/s/ikn36i4vr5t38lf/VOLCS_T_v2.flv?dl=0

Chris Colose 7/19/2016 8:32 PM
 Deleted: S9

Chris Colose 7/23/2016 8:34 PM
 Deleted: S8

Chris Colose 7/23/2016 8:33 PM
 Deleted: https://www.dropbox.com/s/zy8xuh60xso7fvv/VOLCN_P_v2.flv?dl=0

Chris Colose 7/19/2016 8:32 PM
 Deleted: S10

Chris Colose 7/23/2016 8:34 PM
 Deleted: S8

Chris Colose 7/23/2016 8:30 PM
 Deleted: https://www.dropbox.com/s/4mx7qd66f18u21a/VOLCS_P_v2.flv?dl=0

Chris Colose 7/19/2016 8:32 PM
 Deleted: S11

Chris Colose 7/23/2016 8:34 PM
 Deleted: S10

1836
1837
1838

1839

1840

1841

References

Smith, R. D., et al.: The Parallel Ocean Program (POP) reference manual, Ocean component of the Community Climate System Model (CCSM), Tech. Rep. LAUR-10-01853, 141 pp., Los Alamos Natl. Lab., Los Alamos, N. M., 2010.